Title

Dissection of Cell Death Induction by Wheat Stem Rust Resistance Protein Sr35 and Its Matching Effector AvrSr35

Journal

Molecular Plant-Microbe Interactions, 33(2)

ISSN

0894-0282

Authors

Bolus, Stephen
Akhunov, Eduard
Coaker, Gitta
et al.

Publication Date

2020-02-01

DOI

10.1094/mpmi-08-19-0216-r

Peer reviewed

Dissection of cell death induction by wheat stem rust resistance protein Sr35 and its matching effector AvrSr35

Stephen Bolus (1, 2), Eduard Akhunov (3), Gitta Coaker (2)* and Jorge Dubcovsky (1, 4) *

(1) Dept. of Plant Sciences, University of California, Davis, CA 95616, U.S.A.

(2) Dept. of Plant Pathology, University of California, Davis, CA 95616, U.S.A.

(3) Dept. of Plant Pathology, Kansas State University, Manhattan, KS 66506, U.S.A.

(4) Howard Hughes Medical Institute, Chevy Chase, MD 20815, U.S.A.

* Corresponding Authors: Jorge Dubcovsky, E-mail: jdubcovsky@ucdavis.edu and Gitta Coaker, E-mail: glcoaker@ucdavis.edu

Keywords: wheat, barley, stem rust, *Puccinia graminis*, disease resistance, Sr35, nucleotide-binding leucine-rich repeat receptor, effector, AvrSr35, cell death, hypersensitive response.

Funding National Institute for Food and Agriculture, Grant Numbers 2012-67013-19401 and 2017-67007-25939; Howard Hughes Medical Institute. National Science Foundation Graduate Research Fellowship Grant No. 1148897 to S. Bolus. National Institutes of Health Grant R01 GM092772 to G. Coaker.

Abstract

Nucleotide-binding leucine-rich repeat receptors (NLRs) are the most abundant type of immune receptors in plants and can trigger a rapid cell death (hypersensitive) response upon sensing pathogens. We previously cloned the wheat NLR *Sr35*, which encodes a coiled-coil (CC) NLR that confers resistance to the virulent wheat stem rust race Ug99. Here, we investigated Sr35 signaling after *Agrobacterium*-mediated transient expression in *Nicotiana benthamiana.* Expression of Sr35 in *N. benthamiana* leaves triggered a mild cell death response, which is enhanced in the auto-active mutant Sr35 D503V. The N-terminal tagging of Sr35 with GFP blocked the induction of cell death, whereas a C-terminal GFP tag did not. No domain truncations of Sr35 generated cell death responses as strong as the wild-type, but a truncation including the CC-NB-ARC domains in combination with the D503V auto-active mutation triggered cell death. In addition, co-expression of Sr35 with the matching pathogen effector protein AvrSr35 resulted in robust cell-death and electrolyte leakage levels that were similar to auto-active Sr35 and significantly higher than Sr35 alone. Co-expression of Sr35-CC-NB-ARC and AvrSr35 did not induce cell death, confirming the importance of the LRR for AvrSr35 recognition. These findings were confirmed through *Agrobacterium*-mediated transient expression in barley. Taken together, these results implicate the CC-NB-ARC domains of Sr35 in inducing cell death and the LRR domain in AvrSr35 recognition.

Introduction

Plant diseases are a major source of crop losses worldwide (Cesari 2018). An environmentally sustainable approach to reduce these losses is to exploit plants' natural resistance mechanisms (Nelson et al. 2018). Plants have evolved an elaborate innate immune system that relies on receptor-based direct or indirect detection of pathogen features and secreted virulence effector proteins (Thomma et al. 2011). Among the characterized plant resistance genes, the most abundant class are the intracellular nucleotide-binding leucine-rich repeat (NLR) receptors (Dangl et al. 2013). NLR proteins (NLRs) are activated by direct or indirect perception of pathogen effector proteins and are composed of variable N-terminal domains, a conserved nucleotide-binding (NB) domain, and a C-terminal leucine-rich-repeat (LRR) domain (Cesari 2018). A hallmark of NLR activation is a rapid programmed cell death response termed the hypersensitive response (HR) (Chiang and Coaker 2015). However, other NLRs (e.g. wheat *Sr13* and *Sr21*) confer partial resistance by inducing the coordinated expression of multiple pathogenesis-related genes, which slow down infection without triggering an HR response (Zhang et al. 2017; Chen et al. 2018).

NLRs can be assigned to three main groups based on their N-terminal domains: coiled-coil (CC), toll/interleukin-1 receptor-like (TIR), and a basal clade containing CC domains with similarity to RPW8 (CC_R) NLRs (Shao et al. 2016). All plant lineages have CC and CC_R NLRs, whereas several lineages – including monocots - have lost the TIR NLRs (Shao et al. 2016). For CC NLRs, the coiled-coil domain is thought to play an important role in signaling. Indeed, the CC domains of multiple NLR proteins (MLA10, Sr33, Sr50, Rp1-D21, NRG1, ADR1, R3a, N', I2, ZAR1, and Pvr4) are sufficient to induce cell death after transient expression in leaves of *Nicotiana benthamiana* (Bai et al. 2012; Cesari et al. 2016; Wang et al. 2015; Collier et al. 2011;

Hamel et al. 2016; Baudin et al. 2017; Kim et al. 2018). However, there are other NLRs, including RPM1, Rx, Bs2, and RPS5, whose CC domains do not induce cell death in *N. benthamiana* (El Kasmi et al. 2017; Hamel et al. 2016; Ade et al. 2007). The CC domain of ZAR1 contributes to its oligomerization into a wheel-like pentamer (the resistosome) that is implicated in both the induction of cell death and disease resistance (Wang et al. 2019a). Some CC domains also play an important role in targeting NLRs to the cell membrane. For RPS5, alanine substitutions of predicted myristoylation and palmitoylation residues affected RPS5 plasma membrane localization, protein stability, and abolished cell death (Qi et al. 2012). Similarly, mutating two cysteines at an N-terminal predicted palmitoylation site to alanine blocked signaling and disrupted the membrane localization of the rice NLR protein Pit (Kawano et al. 2014).

The NB-ARC (nucleotide binding adaptor shared by APAF-1, R proteins, and CED-4) domain can be divided into three subunits: NB, ARC1, and ARC2 (Sukarta et al. 2016). These regions are thought to cooperate in nucleotide binding and coordinate intra/intermolecular interactions that catalyze the switch between adenosine diphosphate and adenosine triphosphate binding (Collier and Moffett 2009). Upon effector perception, the NB domain of ZAR1 changes conformation and releases ADP to form an intermediate state (Wang et al. 2019b). Within the nucleotide-binding site, mutations in the highly conserved lysine of the P-loop motif (GxxxxGK[T/S]) greatly reduces the ability of NLR proteins to bind ATP and results in a signaling-inactive NLR protein (Tameling et al. 2002). Indeed, this lysine residue was shown to participate directly in ADP and ATP binding for ZAR1 (Wang et al. 2019a; Wang et al. 2019b). In contrast, mutation of the conserved MHD motif to MHV (at the end of the ARC2 subunit) results in constitutively active NLR proteins (Bendahmane et al. 2002). Destabilization of ADP

binding by alteration of the MHD motif may allow for domain re-configurations leading to ATP-binding and activation (Tameling et al 2006).

LRR (leucine-rich repeat) domains are characterized by a repeating pattern of leucine or other hydrophobic amino acids (LxxLxLxxNxL). These repeats in plants fold into a parallel β-sheet and form an arc-shaped structure (Sukarta et al. 2016; Wang et al. 2019b). LRR domains have been implicated in both effector recognition and NLR auto-inhibition; they have hypervariable solvent-exposed amino acid residues, which may facilitate a diversity of intra/intermolecular interactions (Sukarta et al. 2016). Indeed, the LRR domain of ZAR1 was found to play a key role in mediating effector recognition through protein-protein interactions, while also helping to inactivate ZAR1 in the absence of effector detection through intra-molecular interactions (Wang et al. 2019b).

Wheat stem rust, caused by *Puccinia graminis* f. sp. *tritici* (*Pgt*) is a devastating disease. The wheat resistance gene *Sr35* encodes a CC NLR protein that confers near-immunity to Ug99 and related *Pgt* races (Saintenac et al. 2013). The matching effector of Sr35, AvrSr35, is a protein of unknown function, and heterologous co-expression of Sr35 with AvrSr35 induced cell death in *N. benthamiana* (Salcedo et al. 2017). In this work, we characterized the induction of cell death by Sr35 in the presence and absence of AvrSr35 using *Agrobacterium*-mediated transient expression in *N. benthamiana* and *Hordeum vulgare* (barley). We show that overexpression of Sr35 triggers a weak cell death response that is enhanced in the MHD auto-active mutant. No truncation variants of Sr35 were able to signal cell death at wild-type protein levels, but an MHD auto-active Sr35 CC-NB-ARC truncation was able to signal cell death. Sr35 co-expressed with AvrSr35 produced robust cell death, but co-expression of Sr35 CC-NB-ARC

112 truncation with AvrSr35 did not. These results suggest a role of the CC-NB-ARC domains of
113 Sr35 in the induction of cell death and the LRR domain in AvrSr35 recognition.

114

115 ## Results

116 **Overexpression of Sr35 triggers cell death in *Nicotiana benthamiana*.**

117 In order to investigate Sr35 signaling, we sought to develop a system where we could
118 rapidly assess defense signaling from the Sr35 receptor. Transient overexpression of wheat Sr35
119 with a C-terminal GFP tag driven by the 35S promoter in *Agrobacterium*-infiltrated leaves of *N.*
120 *benthamiana* resulted in a weak cell death response that was sometimes difficult to detect
121 macroscopically but was always confirmed in the more sensitive electrolyte leakage experiments
122 described below. A similarly weak response was observed when the Sr35 protein was transiently
123 overexpressed without the GFP tag (Supplementary Fig. S1). In contrast, robust cell death was
124 observed after *N. benthamiana* infiltration with the Sr35 D503V-GFP auto-active MHD mutant
125 (Fig. 1B). Cell death was completely abolished when the GFP tag was placed at the N-terminus,
126 both in the wild-type and auto-active versions of Sr35 (Fig. 1B). No macroscopic cell death was
127 detected in the empty vector and GFP protein controls (Fig. 1B).

128 Macroscopic cell death observations were confirmed and quantified by an electrolyte
129 leakage experiment, which was repeated with similar results (first replicate shown in Fig. 1C and
130 complete statistical analysis in Supplementary Table S2). A combined ANOVA using the two
131 experiments as blocks and the two individual ANOVAs by experiment showed statistically
132 significant effects of the *Sr35* constructs on electrolyte leakage ($P < 0.0001$, Supplementary
133 Table S2). Mean comparisons using the Tukey test at 45 h post infiltration (hpi) showed that the

auto-active Sr35 D503V-GFP construct triggered electrolyte leakage levels more than two-fold higher than the Sr35-GFP construct and 6-fold higher than the other constructs and controls ($P < 0.01$). The electrolyte leakage levels of the Sr35-GFP construct were lower than those using the auto-active Sr35 D503V-GFP construct but were still two-fold higher than the constructs with the N-terminal GFP tag and the negative controls ($P < 0.01$). Collectively, these experiments demonstrate that Sr35 is capable of triggering cell death in *N. benthamiana*, and this function is blocked by addition of GFP to the N-terminus.

In order to verify that all Sr35 proteins were expressed, we performed anti-GFP immunoblots. The results presented in Fig. 1D confirmed that all proteins were expressed at the expected lengths, except for Sr35 D503V-GFP, which was only detectable after immunoprecipitation (Supplementary Fig. S2). We also inferred that a functional Sr35 D503V-GFP protein was present based on the strong cell death response generated by this construct (Fig. 1B). We speculate that the rapid degradation of most cell proteins triggered by the strong cell death response may explain the low levels of protein detected in the Sr35 D503V-GFP auto-active sample.

Truncation variants of Sr35 do not trigger cell death.

To determine the region of Sr35 required for inducing cell death in *N. benthamiana*, we generated constructs overexpressing Sr35 protein domains individually and in different combinations with C-terminal GFP tags (Fig. 2A). Overexpression of the CC domain of Sr35 in *N. benthamiana* with (Fig. 2B) or without (Supplementary Fig. S1) the C-terminal GFP tag showed no macroscopic cell death. Likewise, none of the other Sr35 domains or domain combinations generated macroscopic cell death (Fig. 2B). These results were confirmed by the electrolyte leakage induced by overexpression of these constructs (Supplementary Table S3, Fig.

2C). Highly significant differences ($P < 0.0001$) were detected in the ANOVAs among the different constructs both in the individual experiments and in the combined analysis using experiments as blocks (Supplementary Table S3). Comparisons among electrolyte leakage means using the Tukey tests revealed highly significant differences between the wild-type Sr35 and all the Sr35 truncations ($P < 0.01$) in both the individual experiments and the combined ANOVA (Supplementary Table S3).

In order to verify that Sr35 and the truncation variants were expressed in our constructs, we performed anti-GFP immunoblots. These experiments revealed proteins at the expected sizes; however, cleaved GFP was also observed in Sr35 CC, NB, and CC-NB constructs, possibly due to the relatively high expression levels of these constructs (Fig. 2D). Taken together, these results indicate that truncation of any of the domains from wild-type Sr35 protein abolishes the cell death response observed with the full-length protein.

Sr35 CC-NB-ARC with D503V auto-active mutation is capable of signaling.

To test if the presence of the D503V auto-active mutation could enhance the ability of the truncation variants to induce cell death, we introduced the D503V mutation into the Sr35 NB-ARC, CC-NB-ARC, and NB-ARC-LRR constructs (Fig. 3A). Overexpression of these constructs in *N. benthamiana* revealed that the CC-NB-ARC construct with the D503V auto-active mutation induced macroscopic cell death by 48 hpi (Fig 3B).

Analysis of the electrolyte leakage levels in *N. benthamiana* leaves transiently overexpressing these constructs at 50 hpi revealed significant differences in the ANOVA of two independent experiments and in the combined analysis using experiments as blocks ($P < 0.0001$, Supplementary Table S4). Comparisons among means using a Tukey test ($P <0.01$) showed that the leakage levels induced by the full-length Sr35 D503V protein, the Sr35 CC-NB-ARC D503V

truncation and the Sr35 wild-type were significantly higher than the levels induced by all the other constructs (Fig. 3C, Supplementary Table S4). Among these three constructs, the full-length Sr35 D503V showed the highest electrolyte leakage, but the differences with Sr35 CC-NB-ARC D503V were not significant in any of the analyses. While wild-type Sr35 showed significantly lower leakage values than Sr35 D503V and CC-NB-ARC D503V in the combined ANOVA (P <0.01), the differences in the individual experiments were significant only between Sr35 wild-type and Sr35 D503V (Supplementary Table S4).

Experiments with anti-GFP immunoblots confirmed the presence of proteins of the expected sizes for all constructs (Fig. 3D). There was a clear trend for all three truncated constructs carrying the D503V mutation to accumulate lower protein levels than the corresponding construct without the auto-activating mutation (Fig. 3D). Consistent with the previous result, the complete Sr35 D503V-GFP was only detectable after immunoprecipitation (Supplementary Fig. S2). Altogether, our results indicate that the Sr35 CC-NB-ARC, when coupled with the auto-activating D503V MHD mutation, is sufficient for initiating cell death.

Mutations in predicted palmitoylation residues do not affect signaling.

In a previous study, we showed that Sr35 co-localized with a marker for the endoplasmic reticulum (Salcedo et al. 2017). Since association to cell membranes can be facilitated by the presence of palmitoylation sites, we searched for palmitoylation motifs in Sr35 using the CSS-Palm4.0 prediction website. Two potential palmitoylation sites were detected at cysteine residues 319 (score 2485, threshold 2412) and 649 (score 7315, threshold 3717) in the NB and LRR domains, respectively (Supplementary Fig. S3). We introduced mutations at these positions that resulted in cysteine to alanine substitutions in the wild-type and D503V auto-active Sr35 proteins. The constructs with the mutations in the predicted palmitoylation sites induced

cell death responses similar to their corresponding constructs without the mutations (Supplementary Fig. S3). The empty vector and the Sr35 K206R P-loop mutant, included as negative controls, showed no induction of cell death (Supplementary Fig. S3).

Individual ANOVAs and a combined ANOVA, where two individual experiments were analyzed as blocks, revealed significant differences in the *Sr35* constructs tested for electrolyte leakage ($P < 0.0001$, Supplementary Fig. S3 and Supplementary Table S5). As in previous experiments, the two constructs with the D503V auto-activating mutations showed significantly higher electrolyte leakage levels (Tukey test $P < 0.01$, Supplementary Table S5) than all other constructs in both single experiment and combined ANOVAs. The wild-type constructs (with and without the mutations at the putative palmitoylation sites) showed significantly higher leakage levels than the empty vector and K206R P-loop mutant in both single experiment and combined ANOVAs (>3-fold higher, Tukey test $P < 0.01$, Supplementary Table S5).

Anti-GFP immunoblots confirmed the expression of proteins of the expected sizes (Supplementary Fig. S3). The complete constructs with the auto-active mutation (D503V and C319A/C649A/D503V) were not detected in the anti-GFP immunoblots but were detected after immunoprecipitation (Supplementary Fig. S2).

Sr35 induces cell death in barley.

It has been shown recently that Sr35 can confer resistance to *Pgt* in barley (Hatta et al. 2018). Using a method for *Agrobacterium*-infiltration described previously (Lu et al. 2016), we tested our constructs for signs of macroscopic cell death in barley. Similar to observations in *N. benthamiana*, Sr35 D503V-GFP induced a consistent cell death response in barley but GFP-Sr35 D503V did not (Fig. 4). However, macroscopic cell death was not observed in barley for the wild-type Sr35-GFP construct as it was in *N. benthamiana* infiltrated with the same bacterial

culture (Fig. 4). Sr35 CC-NB-ARC D503V-GFP did not induce as strong as a cell death response in barley as in *N. benthamiana*, but several of the infiltrated leaves (4/20) showed signs of macroscopic cell death (Fig. 4), and this result was reproducible between experiments. This could be due to differences in protein expression levels between the two systems, because the 35S promoter used in these experiments is more effective in dicot than monocot species (Christensen et al. 1992). Similar to the results observed in *N. benthamiana*, GFP, Sr35 CC-GFP, Sr35 K206R, and Sr35 NB-ARC-LRR D503V-GFP did not trigger cell death in barley (Fig. 4). These results suggest that Sr35 exhibits similar signaling mechanisms in both monocots and dicots.

AvrSr35-induced cell death is restricted to C-terminally tagged, full-length Sr35 protein

Sr35 and AvrSr35 were previously shown to trigger cell death when co-expressed in *N. benthamiana* (Salcedo et al. 2017). To test if the CC-NB-ARC truncation is capable of inducing cell death in the presence of AvrSr35, we co-expressed Sr35 CC-NB-ARC-GFP, Sr35-GFP, and GFP-Sr35 with an AvrSr35 protein that lacked the signal peptide and included a C-terminal monomeric Red Fluorescent Protein (mRFP) tag (AvrSr35-SP+mRFP, Fig 5A). We included Sr35 D503V-GFP as a positive control. Full-length Sr35-GFP co-expressed with AvrSr35-SP+mRFP induced macroscopic cell death reactions similar to those observed in auto-active Sr35 D503V-GFP in *N. benthamiana* (Fig. 5B). Sr35-GFP, when expressed alone, induced a mild cell death response, and no macroscopic effects were detected for the other constructs.

In order to quantify and compare cell death responses, statistical analyses were performed on electrolyte leakage data collected at 50 hpi (Fig. 5C). Significant effects were detected in the combined ANOVA using the two individual experiments as blocks, as well as in the two individual ANOVAs ($P < 0.0001$, Supplementary Table S6). Mean comparisons using

Tukey tests ($P < 0.01$) showed that co-expression of Sr35-GFP and AvrSr35-SP+mRFP induced electrolyte leakage levels that were not significantly different from the auto-active Sr35 D503V-GFP alone or the auto-active Sr35 D503V-GFP co-expressed with AvrSr35-SP+mRFP (Fig. 5C). These constructs induced significantly higher electrolyte leakage levels than all other constructs in both individual and combined analyses ($P < 0.01$). Sr35-GFP alone induced lower electrolyte leakage levels than the auto-active constructs and Sr35-GFP co-infiltrated with AvrSr35-SP+mRFP ($P < 0.01$), but was significantly higher ($P < 0.01$) than all other constructs in both the individual and combined analyses ($P < 0.01$, Fig. 5C, Supplementary Table S6).

Sr35 proteins were expressed at the expected sizes as revealed in an anti-GFP immunoblot (Fig. 5D). The same protein samples were tested for AvrSr35-SP+mRFP using anti-DsRed immunoblot. AvrSr35-SP+mRFP was expressed in co-infiltration samples as expected (Fig. 5D). However, AvrSr35-SP+mRFP was hardly detected when co-infiltrated with Sr35 D503V-GFP, likely due to rapid cell death. As before, Sr35 D503V-GFP was only detected after immunoprecipitation (Supplementary Fig. S2).

To test the effect of co-expression of AvrSr35 and Sr35 in barley using *Agrobacterium*-mediated transient expression, we cloned AvrSr35-SP downstream of a maize *UBIQUITIN* promoter and upstream of a 3xHA tag (Fig 6A). Co-expression of Sr35-GFP with AvrSr35-SP+3xHA in barley resulted in macroscopic cell death in 10 out of the 20 leaves tested from different plants (Fig. 6B), whereas the auto-active construct Sr35 D503V-GFP with and without AvrSr35-SP+3xHA induced cell death in all 20 leaves tested. Macroscopic cell death was not observed for GFP-Sr35 and Sr35 CC-NB-ARC with and without AvrSr35-SP+3xHA (Fig. 6B). As controls, AvrSr35-SP+mRFP and Sr35-GFP over-expressed alone did not trigger cell death (Fig. 6B). For comparison, leaves of *N. benthamiana* were infiltrated with the same bacterial

cultures as barley. Macroscopic cell death was consistent between *N. benthamiana* and barley, except for Sr35-GFP, where a weak cell death was observed only in *N. benthamiana* (Fig. 6B). AvrSr35-SP+3xHA expression was tested in *N. benthamiana* using an anti-HA immunoblot. The AvrSr35 protein was expressed at the expected size (Fig. 6C).

Taken together, these results confirmed that AvrSr35 is able to induce activation of Sr35 in *N. benthamiana*, and we extended this observation to barley. In addition, we show that Sr35 recognition of AvrSr35 and the subsequent induction of cell death is dependent on the presence of the LRR domain and is blocked by a GFP tag on the N-terminus of the Sr35 protein.

Discussion

The results presented in this study provide evidence that Sr35 is capable of inducing cell death in the presence of the matching AvrSr35 effector in both *N. benthamiana* and barley. Furthermore, we identified truncation variants and point mutations in the Sr35 protein that enhanced or reduced its ability to trigger cell death.

Point mutations and fusion tags affecting the ability of Sr35 to signal cell death

The difference between the mild cell death response induced by the wild-type Sr35 construct (Fig. 1B) and the strong cell death response observed with the co-infiltration of Sr35 and AvrSr35 (Fig. 5B) suggests that the wild-type Sr35 protein is present mainly in an inactive state and can be activated by the AvrSr35 effector in a heterologous system. The mild electrolyte leakage induced by the wild-type construct may be the result of the strong overexpression of Sr35 driven by the 35S promoter in *N. benthamiana*. This overexpression could result in the accumulation and auto-activation of Sr35 proteins due to improper intra/intermolecular

interactions. The 35S promoter used to overexpress Sr35 protein in *N. benthamiana* is less effective in monocots (Christensen et al. 1992), which may explain the absence of a macroscopic cell death response when the same construct was used to express Sr35 in barley leaves (Fig. 4).

The hypothesis that the Sr35 protein in *N. benthamiana* and barley is mainly present in an inactive state is supported by the stronger hypersensitive response observed in both species when the auto-activating mutation D503V is incorporated into the Sr35 full-length constructs (Figs. 1 and 4). The MHD to MHV mutation results in constitutively active NLR proteins from many plant species (Bendahmane et al. 2002; Tameling et al. 2006; Gao et al. 2011; Bai et al. 2012; Kawano et al. 2014). In contrast, the Sr35 P-loop mutant K206R reduced cell death triggered by the overexpression of Sr35 in *N. benthamiana* (Supplementary Fig. S3). This is consistent with other findings that mutation of the conserved lysine in the P-loop motif to arginine leads to NLR inactivation (Tameling et al. 2006; Bai et al. 2012). Mutation of two predicted palmitoylation motifs in Sr35 protein did not affect cell death responses of WT or auto-active proteins (Supplementary Fig. S3), suggesting that either they were not real palmitoylation sites or that their presence is not essential for inducing cell death. This was contrary to what was observed in Pit, a rice NLR protein conferring resistance to the blast fungus, where mutation of the two predicted palmitoylation motifs in the CC domain led to inactivation of the NLR protein (Kawano et al. 2014).

Both Sr35 and Sr35 D503V auto-active constructs lost their ability to signal cell death in *N. benthamiana* (Fig. 1) and barley (Fig. 4) when a GFP tag was added to the N-terminal domain, but not when it was added to the C-terminal domain. A similar loss-of-function when a tag was fused to the N-terminus but not when it was fused to the C–terminus was reported for Pit (Kawano et al. 2014), ZAR1 (Wang et al. 2019a) and both MLA1 and MLA6 (Bieri et al. 2004).

317 In contrast, RPM1 was still able to trigger cell death with the addition of an N-terminal CBL
318 membrane-targeting tag (Gao et al. 2011). The addition of an N-terminal tag may affect the
319 ability of these NLRs to function properly by interfering with their ability to associate with
320 membranes. Indeed, the addition of an N-terminal tag to Pit changed its localization from
321 membrane-associated to cytosolic (Kawano et al. 2014), and changes in the CC domain leading
322 to membrane-localization and subsequent NLR activation was important for oligomerization and
323 cell death in the CC NLR ZAR1 (Wang et al. 2019a).

324 **Ability of different Sr35 domains and domain combinations to signal cell death**

325 The ability of an N-terminal tag to suppress Sr35 induction of cell death indicates that the
326 N-terminal CC domain may play an important role in this process. Our experiments using
327 different Sr35 truncated proteins were consistent with this hypothesis. The truncation of the CC
328 domain from the complete Sr35 D503V auto-active mutant eliminated the strong HR and high
329 electrolyte leakage levels induced by this construct (Fig. 3B). Similarly, the CC-NB-ARC
330 D503V construct lost its ability to induce cell death when the CC domain was not included in the
331 construct (Fig. 3B). These results, together with the inability of the CC domain alone to induce
332 cell death in the leaves of *N. benthamiana* (Fig. 2B), suggest that the CC domain of Sr35 plays a
333 critical role in the induction of cell death but is not sufficient to induce this response.

334 No Sr35 truncation was able to match the strength of cell death triggered by the full-
335 length Sr35 in *N. benthamiana* (Fig. 2). Several domains or domain combinations that were
336 sufficient to induce cell death in other CC-NLR proteins were not effective for Sr35. For
337 example, the CC-NB construct was not able to induce cell death in Sr35 but was sufficient to
338 induce HR for Rx, MLA10, Sr33, and Sr50 (Rairdan et al. 2008; Bai et al. 2012; Cesari et al.
339 2016). Similarly, the CC-NB-ARC domain combination was unable to trigger cell death in Sr35

but was effective for RPS5, MLA10, and Pvr4 (Ade et al. 2007; Bai et al. 2012; Kim et al. 2018). However, we observed a strong cell death signal for the Sr35 CC-NB-ARC D503V auto-active construct, whereas the same domain and mutant combination was not effective for RPM1 (El Kasmi et al. 2017). This result suggests that the CC-NB-ARC domains are sufficient to generate active folding of the Sr35 protein, but this is not a universal phenomenon for CC containing NLRs.

Sr35 requires the LRR domain to signal cell death in response to AvrSr35

Although the auto-active mutant Sr35 CC-NB-ARC D503V truncation was able to induce cell death (Fig. 3B), co-expression of Sr35 CC-NB-ARC with AvrSr35 did not result in cell death in both *N. benthamiana* (Fig. 5) and barley (Fig. 6). This finding implicates the LRR domain in AvrSr35 recognition but decouples recognition from Sr35 signaling activity. An N-terminal tag on the Sr35 protein was able to block the induction of cell death in the presence of AvrSr35 (Fig. 5B). This was consistent with the previous finding that Sr35 D503V with an N-terminal GFP tag is not capable of triggering cell death (Fig. 1B). Therefore, our current model is that Sr35 is activated (directly or indirectly) by AvrSr35 through its LRR domain and that this recognition leads to changes in the CC-NB-ARC domains that facilitate signaling. This model is consistent with the observation that the *in planta* interaction between AvrSr35 and Sr35 is negatively affected by three amino acid substitutions at positions 854, 856 and 858 in the LRR domain of Sr35 and the susceptibility of this mutant to the Ug99 race of stem rust pathogen (Salcedo et al., 2017; Saintenac et al. 2013). The importance of the distal region of the LRR in pathogen recognition is also supported by an induced mutation (W856*) that eliminates the last 63 amino acids of the Sr35 LRR and results in susceptible plants (Saintenac et al. 2013).

Materials and Methods

Plasmid Construction

The *T. monococcum* Sr35 genomic sequence without a stop codon was PCR amplified from a clone previously used in transgenic complementation experiments (Saintenac et al. 2013) using Phusion polymerase (New England BioLabs) and primers Sr35gateway_F/R (Supplementary Table S1). Sr35 CC, CC-NB, CC-NB-ARC, NB, NB-ARC, NB-ARC-LRR, and LRR fragments were PCR amplified from the same genomic clone using primer pairs Sr35gateway_F/Sr35CCgatewayR, Sr35gateway_F/Sr35NBgateway_R, Sr35gateway_F/Sr35ARCgateway_R, Sr35NBgateway_F/Sr35NBgateway_R, Sr35NBgateway_F/Sr35ARCgateway_R, Sr35NBgatewayF/Sr35gateway_R, and Sr35LRRgateway_F/Sr35gateway_R, respectively (Supplementary Table S1). PCR products were inserted into Gateway pDONR/Zeo vector using Gateway BP Clonase II enzyme mix (ThermoFisher).

Single and multiple mutation constructs were made using PCR site-directed mutagenesis and, if necessary, multiple rounds of PCR site-directed mutagenesis on pDONR constructs. The CSS-Palm 4.0 Server (Ren et al. 2008) was used to predict the putative palmitoylation sites, and Sr35PCR primers Sr35C319A_F/ R and Sr35C649A_F/ R (Supplementary Table S1) were used to induce mutations to replace the cysteines in the predicted palmitoylation sites with alanines. The D503V auto-active mutant and the K206R P-loop mutant constructs were generated using PCR primer sets Sr35D503V_F/R and Sr35K206R_F/R, respectively (Supplementary Table S1). C-terminal stop codons in Sr35 and Sr35 CC constructs were generated with primer pair Sr35gateway_F/Sr35_TGA_gateway_R and Sr35gateway_F/Sr35CC_TGA_gateway_R (Supplementary Table S1). For all constructs, mutations were verified by Sanger sequencing.

Sr35 and Sr35 D503V were transferred to the pGWB5 (GFP-C-terminal) and pGWB6 (GFP-N-terminal) destination binary vectors (Nakagawa et al. 2007) using Gateway LR Clonase II enzyme mix (ThermoFisher). All other constructs were transferred to the pGWB5 vector only.

pSITE4NA AvrSr35(-SP)+mRFP construct was kindly provided by Dr. Eduard Akhunov (Salcedo et al. 2017) and verified by Sanger sequencing. The AvrSr35 without the signal peptide (AvrSr35-SP) in pLC41HA construct was made by first amplifying AvrSr35(-SP) with primers AvrSr35gateway_F/R (Supplementary Table S1). The resulting PCR product was inserted into Gateway pDONR/Zeo vector using Gateway BP Clonase II enzyme mix (ThermoFisher). The construct sequence was verified by Sanger sequencing and transferred downstream the maize UBIQUITIN promoter and upstream a 3xHA tag in a modified, gateway-compatible pLC41 (Japan Tobacco) destination binary vector using LR Clonase II enzyme mix (ThermoFisher).

Transient expression in *Nicotiana benthamiana*

Nicotiana benthamiana plants were grown for 3 weeks in growth chambers at 25 ºC with 85 % humidity and 16 h of 100 µmol/s*m^2 light. *Agrobacterium tumefaciens* strain EHA105 bacteria were transformed with pGWB5 and pGWB6 *Sr35* constructs. Transformed *A. tumefaciens* were cultured overnight at 28 °C in LB broth containing 50 µg/mL kanamycin and 100 µg/mL rifampicin. Bacteria were pelleted by centrifugation and re-suspended in infiltration media (1.15 x Murashige and Skoog basal salts, 58 mM sucrose, 10 mM MES (pH 5.6), and 200 µmol acetosyringone). *A. tumefaciens* culture density was then adjusted to $O.D._{600}$ 0.5 and incubated with shaking at room temperature for at least 1 h prior to infiltration in *N. benthamiana* leaves using a 1 mL tuberculin syringe. For Sr35-AvrSr35 co-infiltration experiments, *A. tumefaciens* cultures were adjusted to $O.D._{600}$ 1.0 for each construct, then mixed 1:1 with another construct or infiltration media ($O.D._{600}$ 0.5 for each construct after mixing).

After *Agrobacterium* infiltration, *N. benthamiana* plants were placed at room temperature under constant 30 µmol/s*m^2 light. Leaf tissue for electrolyte leakage was harvested starting at 15 or 20 h post infiltration (hpi). Leaf tissue for protein extraction was sampled 24 hpi, and leaves for macroscopic cell death were sampled and imaged at 48 hpi.

Electrolyte Leakage Assay

To quantify cell death, leaf discs (0.79 cm^2) of *Agrobacterium*-infiltrated *N. benthamiana* leaves were made using a cork borer and placed as pairs (two subsamples from the same leaf) in 12 well tissue culture plates (VWR) with 5 mL distilled water for 30 minutes. Four biological replicates (an individual, *Agrobacterium*-infiltrated leaf on an individual *N. benthamiana* plant) were made for each *Agrobacterium* culture. Water was replaced with 5 mL of new distilled water, and electrolyte leakage was monitored using a Model 3200 conductance instrument (YSI) every 5 hours from 15 to 45, or 20 to 50 hpi. Leaf discs were kept at room temperature under constant 30 µmol/s*m^2 light until electrolyte leakage measurements were conducted.

Statistical analyses were performed using the electrolyte leakage (µS/cm) data from the last time point collected. Normality of residuals was tested with the Shapiro-Wilk test and homogeneity of variances with the Levene's test. If necessary, data were transformed using different power transformations to satisfy the ANOVA assumptions. Means were compared against each other using Tukey's honestly significant difference (HSD) test using alpha = 0.01 for all tests. All electrolyte leakage experiments were repeated at least once, and the two experiments were analyzed both separately and in a combined ANOVA using experiments as blocks. All statistical analysis were performed using SAS version 9.4.

Protein analyses

Protein was extracted from 0.2 g of flash-frozen *Nicotiana benthamiana* leaf tissue collected 24 hours post *Agrobacterium* infiltration by grinding under liquid nitrogen with a mortar and pestle and adding 400 µL of extraction buffer [50 mM Tris-HCl pH 7.4, 150 mM NaCl, 10 mM EDTA (pH 8.0), 10 mM DTT, 0.2 % Triton X-100, 0.5 % (w/v) polyvinylpyrrolidone, 1:100 protease inhibitor cocktail (Sigma P9599), and 1mM PMSF]. The lysate was cleared by centrifuging at 12,000 x g for 10 minutes at 4°C. Supernatant was collected, transferred to a new 1.5 mL tube, and centrifuged again at 12,000 x g for 10 min at 4 °C. The final supernatant was collected and denatured at 65 °C for 10 min in 1 x Laemmli (-Bromophenol Blue). The total protein was quantified using the Pierce 660 nm protein assay with the addition of the Ionic Detergent Compatibility Reagent (Thermo Fisher).

Twenty µg of protein for each sample were loaded and resolved on a 10 % SDS/PAGE gel. Proteins were then transferred to a PVDF membrane overnight at 30 V. Membranes were washed with TBST and blocked with 5 % Blotting-Grade Blocker (BioRad) in TBST. A dilution of 1:5000 anti-GFP-HRP (Miltenyi Biotec 130-091-833) antibody was used to detect GFP and GFP fusion proteins. 1:1000 αDsRed (Santa Cruz Biotechnology sc-390909) and 1:25,000 anti-Mouse IgG-HRP (Sigma-Aldrich A9044) antibodies were used to detect AvrSr35-mRFP fusion protein, and 1:10,000 anti-HA-HRP (Roche 12013819001) antibody was used to detect AvrSr35-HA fusion protein. Blots were imaged using SuperSignal West Femto Maximum Sensitivity Substrate (Thermo Fisher) and a ChemiDoc (BioRad).

For full-length, auto-active *Sr35* constructs, the encoded protein was immunoprecipitated to facilitate detection. Protein was extracted from 0.5 g of flash-frozen *Agrobacterium*-infiltrated *Nicotiana benthamiana* leaf tissue by grinding under liquid nitrogen with a mortar and pestle and adding 1 mL of extraction buffer (same as described previously). The lysate was cleared by

centrifuging at 12,000xg for 10 min at 4 °C. Supernatant was collected, transferred to a new 1.5 mL tube, and centrifuged again at 12,000 x g for 10 min at 4 °C. GFP-Trap_A beads (ChromoTec) were washed twice by adding 1 mL extraction buffer (without polyvinylpyrrolidone) then pelleting by centrifugation at 1,000 x g for 2 min. Seven hundred µL of the final protein supernatant was combined with 20 µL of the washed beads and turned end-over-end at 4 °C for 2 hours. From the final supernatant, 37.5 µL was retained as loading control. Beads were collected by centrifuging at 1,000 x g for 2 min. Flow-through was discarded, and beads were washed three times with 1 mL extraction buffer (without polyvinylpyrrolidone). Proteins were eluted from beads by heating at 65 °C for 10 min in 1 x Laemmli buffer. Loading samples were also denatured in this way. Samples were separated by SDS/PAGE and processed for GFP immunodetection as described above.

Ponceau S stain was used to visualize Rubisco's large subunit protein across protein samples. Blots were stained with a Ponceau S/acetic acid solution [0.1 % (w/v) Ponceau S (MP Biomedicals) and 5% (v/v) acetic acid] for 5 minutes. Blots were then rinsed with distilled water until bands were clearly visible and background was appropriately reduced. The stained blots were imaged using a ChemiDoc (BioRad).

Transient expression in barley

Agrobacterium-mediated transient expression in barley leaves was performed as described previously (Lu et al. 2016). Manchuria barley (*Hordeum vulgare* L. cultivar Manchuria) plants were grown in a growth chamber for 2 weeks at 23 °C with 10 h of 100 µmol/s*m^2 light. *Nicotiana benthamiana* (control) plants were grown for 3 weeks in growth chambers at 25 ºC with 85 % humidity and 16 h of 100 µmol/s*m^2 light. *Agrobacterium tumefaciens* strain AGL1 were transformed with *Sr35* and *AvrSr35* constructs. Fresh *Agrobacterium* cultures were grown

477 overnight at 28 °C in LB broth containing 50 µg/mL kanamycin, 100 µg/mL ampicillin, and 100
478 µg/mL rifampicin. Bacterial cultures were pelleted by centrifugation, re-suspended in infiltration
479 buffer (10 mM MES (pH 5.6), 10 mM $MgCl_2$, and 400 µmol acetosyringone), and adjusted to a
480 final $O.D._{600}$ of 2.0. For Sr35-AvrSr35 co-infiltration experiments, each culture was adjusted to
481 $O.D._{600}$ of 2.0 and mixed in a 1:1 ratio. *Agrobacterium* were syringe infiltrated into the second
482 leaf of 12-day-old barley plants and into leaves of *N. benthamiana* as a positive control. After
483 *Agrobacterium* infiltration, barley and *N. benthamiana* plants were placed at room temperature
484 under constant 30 µmol/s*m^2 light. *N. benthamiana* leaves were harvested and imaged at 48 or
485 72 hpi for macroscopic cell death observations. For each construct, 20 leaves from 20 individual
486 barley plants were harvested and imaged 7 days post infiltration for macroscopic cell death
487 observation.

488

489 Acknowledgements

490 This project was supported by the Agriculture and Food Research Initiative Competitive
491 Grants 2012-67013-19401 and 2017-67007-25939 from the USDA National Institute of Food
492 and Agriculture to J.D., National Institute of Health grant R01 GM092772 to G.C., and National
493 Science Foundation Graduate Research Fellowship Grant No. 1148897 to S.B. The authors thank
494 Elizabeth Henry and Tanya Chilcote for excellent technical assistance and Meixiang Zhang for
495 helpful discussion. The authors also thank Takaki Maekawa, Simone Gieraths, and Paul Schulze-
496 Lefert for their assistance with the barley *Agro*-infiltration experiments and Brande Wulff, Brian
497 Steffenson, and Asyraf Hatta for sharing unpublished data on the effectiveness of Sr35 in barley.

498

Literature cited

Ade, J., DeYoung, B. J., Golstein, C., and Innes, R. W. 2007. Indirect activation of a plant nucleotide binding site-leucine-rich repeat protein by a bacterial protease. Proc. Natl. Acad. Sci. 104:2531–2536.

Bai, S., Liu, J., Chang, C., Zhang, L., Maekawa, T., Wang, Q., Xiao, W., Liu, Y., Chai, J., Takken, F. L. W., Schulze-Lefert, P., and Shen, Q. H. 2012. Structure-function analysis of barley NLR immune receptor MLA10 reveals its cell compartment specific activity in cell death and disease resistance. PLoS Pathog. 8:21–25.

Baudin, M., Hassan, J. A., Schreiber, K. J., and Lewis, J. D. 2017. Analysis of the ZAR1 immune complex reveals determinants for immunity and molecular interactions. Plant Physiol. 174:2038-2053.

Bendahmane, A., Farnham, G., Moffett, P., and Baulcombe, D. C. 2002. Constitutive gain-of-function mutants in a nucleotide binding site-leucine rich repeat protein encoded at the *Rx* locus of potato. Plant J. 32:195–204.

Bieri, S., Mauch, S., Shen, Q.-H., Peart, J., Devoto, A., Casais, C., Ceron, F., Schulze, S., Steinbiß, H.-H., Shirasu, K., and Schulze-Lefert, P. 2004. RAR1 positively controls steady state levels of barley MLA resistance proteins and enables sufficient MLA6 accumulation for effective resistance. Plant Cell. 16:3480-3495.

Cesari, S. 2018. Multiple strategies for pathogen perception by plant immune receptors. New Phytol. 219:17–24.

519 Cesari, S., Moore, J., Chen, C., Webb, D., Periyannan, S., Mago, R., Bernoux, M., Lagudah, E.
520 S., and Dodds, P. N. 2016. Cytosolic activation of cell death and stem rust resistance by
521 cereal MLA-family CC–NLR proteins. Proc. Natl. Acad. Sci. 113:10204–10209.

522 Chen, S., Zhang, W., Bolus, S., Rouse, M. N., and Dubcovsky, J. 2018. Identification and
523 characterization of wheat stem rust resistance gene *Sr21* effective against the Ug99 race
524 group at high temperature. PLOS Genet. 14:e1007287.

525 Chiang, Y.-H., and Coaker, G. 2015. Effector triggered immunity: NLR immune perception and
526 downstream defense responses. Arab. B. 13:e0183.

527 Christensen, A. H., Sharrock, R. A., and Quail, P. H. 1992. Maize polyubiquitin genes: structure,
528 thermal perturbation of expression and transcript splicing, and promoter activity following
529 transfer to protoplasts by electroporation. Plant Mol. Biol. 18:675–689.

530 Collier, S. M., Hamel, L.-P., and Moffett, P. 2011. Cell death mediated by the N-terminal
531 domains of a unique and highly conserved class of NB-LRR protein. Mol. Plant-Microbe
532 Interact. 24:918–931.

533 Collier, S. M., and Moffett, P. 2009. NB-LRRs work a “bait and switch” on pathogens. Trends
534 Plant Sci. 14:521–529.

535 Dangl, J. L., Horvath, D. M., and Staskawicz, B. J. 2013. Pivoting the plant immune system from
536 dissection to deployment. Science. 341:746-751.

537 El Kasmi, F., Chung, E.-H., Anderson, R. G., Li, J., Wan, L., Eitas, T. K., Gao, Z., and Dangl, J.
538 L. 2017. Signaling from the plasma-membrane localized plant immune receptor RPM1
539 requires self-association of the full-length protein. Proc. Natl. Acad. Sci. 114:7385-7394.

Gao, Z., Chung, E.-H., Eitas, T. K., and Dangl, J. L. 2011. Plant intracellular innate immune receptor resistance to *Pseudomonas syringae* pv. 1 (RPM1) is activated at, and functions on, the plasma membrane. Proc. Natl. Acad. Sci. 108:7619-7624.

Hamel, L.-P., Sekine, K.-T., Wallon, T., Sugiwaka, Y., Kobayashi, K., and Moffett, P. 2016. The chloroplastic protein THF1 interacts with the coiled-coil domain of the disease resistance protein N′ and regulates light-dependent cell death. Plant Physiol. 171:658–674.

Hatta, M. A., Johnson, R., Matny, O., Smedley, M. A., Yu, G., Mago, R., Lagudah, E. S., Patron, N., Ayliffe, M., Rouse, M. N., Wendy, A., Periyannan, S. K., Steffenson, B. J., and Wulff, B. B. H. 2018. The wheat *Sr22*, *Sr33*, *Sr35* and *Sr45* genes confer resistance against stem rust in barley. bioRxiv 374637.

Kawano, Y., Fujiwara, T., Yao, A., Housen, Y., Hayashi, K., and Shimamoto, K. 2014. Palmitoylation-dependent membrane localization of the rice resistance protein Pit is critical for the activation of the small GTPase OsRac1. J. Biol. Chem. 289:19079–19088.

Kim, S.-B., Lee, H.-Y., Choi, E.-H., Park, E., Kim, J.-H., Moon, K.-B., Kim, H.-S., and Choi, D. 2018. The coiled-coil and leucine-rich repeat domain of the potyvirus resistance protein Pvr4 has a distinct role in signaling and pathogen recognition. Mol. Plant-Microbe Interact. 31:906–913.

Lu, X., Kracher, B., Saur, I. M. L., Bauer, S., Ellwood, S. R., Wise, R., Yaeno, T., Maekawa, T., and Schulze-Lefert, P. 2016. Allelic barley MLA immune receptors recognize sequence-unrelated avirulence effectors of the powdery mildew pathogen. Proc. Natl. Acad. Sci. 113:6486–6495.

561 Nakagawa, T., Kurose, T., Hino, T., Tanaka, K., Kawamukai, M., Niwa, Y., Toyooka, K.,
562 Matsuoka, K., Jinbo, T., and Kimura, T. 2007. Development of series of gateway binary
563 vectors, pGWBs, for realizing efficient construction of fusion genes for plant
564 transformation. J. Biosci. Bioeng. 104:34–41.

565 Nelson, R., Wiesner-Hanks, T., Wisser, R., and Balint-Kurti, P. 2018. Navigating complexity to
566 breed disease-resistant crops. Nat. Rev. Genet. 19:21–33.

567 Qi, D., DeYoung, B. J., and Innes, R. W. 2012. Structure-function analysis of the coiled-coil and
568 leucine-rich repeat domains of the RPS5 disease resistance protein. Plant Physiol.
569 158:1819–1832.

570 Rairdan, G. J., Collier, S. M., Sacco, M. A., Baldwin, T. T., Boettrich, T., and Moffett, P. 2008.
571 The coiled-coil and nucleotide binding domains of the potato Rx disease resistance protein
572 function in pathogen recognition and signaling. Plant Cell. 20:739–751.

573 Ren, J., Wen, L., Gao, X., Jin, C., Xue, Y., and Yao, X. 2008. CSS-Palm 2.0: An updated
574 software for palmitoylation sites prediction. Protein Eng. Des. Sel. 21:639–644.

575 Saintenac, C., Zhang, W., Salcedo, A., Rouse, M. N., Trick, H. N., Akhunov, E., and Dubcovsky,
576 J. 2013. Identification of wheat gene *Sr35* that confers resistance to Ug99 stem rust race
577 group. Science. 341:783-786.

578 Salcedo, A., Rutter, W., Wang, S., Akhunova, A., Bolus, S., Chao, S., Anderson, N., De Soto, M.
579 F., Rouse, M., Szabo, L., Bowden, R. L., Dubcovsky, J., and Akhunov, E. 2017. Variation
580 in the *AvrSr35* gene determines *Sr35* resistance against wheat stem rust race Ug99. Science.
581 358:1604–1606.

582 Shao, Z.-Q., Xue, J.-Y., Wu, P., Zhang, Y.-M., Wu, Y., Hang, Y.-Y., Wang, B., and Chen, J.-Q.
583 2016. Large-scale analyses of angiosperm nucleotide-binding site-leucine-rich repeat genes
584 reveal three anciently diverged classes with distinct evolutionary patterns. Plant Physiol.
585 170: 2095–2109.

586 Sukarta, O. C. A., Slootweg, E. J., and Goverse, A. 2016. Structure-informed insights for NLR
587 functioning in plant immunity. Semin. Cell Dev. Biol. 56:134–149.

588 Tameling, W. I. L., Elzinga, S. D. J., Darmin, P. S., Vossen, J. H., Takken, F. L. W., Haring, M.
589 A., and Cornelissen, B. J. C. 2002. The tomato *R* gene products I-2 and Mi-1 are functional
590 ATP binding proteins with ATPase activity. Plant Cell. 14:2929-2939.

591 Tameling, W. I. L., Vossen, J. H., Albrecht, M., Lengauer, T., Berden, J. A., Haring, M. A.,
592 Cornelissen, B. J. C., and Takken, F. L. W. 2006. Mutations in the NB-ARC domain of I-2
593 that impair ATP hydrolysis cause autoactivation. Plant Physiol. 140:1233-1245.

594 Thomma, B. P. H. J., Nürnberger, T., and Joosten, M. H. A. J. 2011. Of PAMPs and effectors:
595 the blurred PTI-ETI dichotomy. Plant Cell. 23:4–15.

596 Wang, G. F., Ji, J., EI-Kasmi, F., Dangl, J. L., Johal, G., and Balint-Kurti, P. J. 2015. Molecular
597 and functional analyses of a maize autoactive NB-LRR protein identify precise structural
598 requirements for activity. PLoS Pathog. 11:1–32.

599 Wang, J., Hu, M., Wang, J., Qi, J., Han, Z., Wang, G., Qi, Y., Wang, H.-W., Zhou, J.-M., and
600 Chai, J. 2019a. Reconstitution and structure of a plant NLR resistosome conferring
601 immunity. Science. 364:eaav5870.

602 Wang, J., Wang, J., Hu, M., Wu, S., Qi, J., Wang, G., Han, Z., Qi, Y., Gao, N., Wang, H.-W.,
603 Zhou, J.-M., and Chai, J. 2019b. Ligand-triggered allosteric ADP release primes a plant
604 NLR complex. Science. 364:eaav5868.

605 Zhang, W., Chen, S., Abate, Z., Nirmala, J., Rouse, M. N., and Dubcovsky, J. 2017.
606 Identification and characterization of *Sr13*, a tetraploid wheat gene that confers resistance to
607 the Ug99 stem rust race group. Proc. Natl. Acad. Sci. 114:9483–9492.

608 **Figure legends**

609 **Figure 1**. Sr35 induces cell death when overexpressed in *Nicotiana benthamiana*. **A,** Schematic
610 diagram of GFP fused to the N-terminus (GFP-Sr35) and C-terminus (Sr35-GFP) of Sr35 with
611 and without the auto-active mutation (D503V). **B,** Macroscopic cell death observed 48 hours
612 post infiltration (hpi) with *Agrobacterium*. ev = empty vector. **C,** Electrolyte leakage 15 to 45
613 hpi. Error bars represent standard error based on four biological replicates per construct.
614 Different letters indicate significantly different groups of means based on Tukey's HSD test (α =
615 0.01) performed at 45 hpi (statistical analyses in Supplementary Table S2). **D,** Western blots of
616 protein extracts from *N. benthamiana* 24 hpi analyzed using an anti-GFP-HRP antibody. No
617 protein was observed here for Sr35 D503V-GFP, but it was detected after immunoprecipitation
618 (Supplementary Fig. S2). The lower panel is the same blot stained with Ponceau S to reveal
619 Rubisco's large subunit protein used as loading control.

620 **Figure 2**. Truncation variants of Sr35 are not able to induce cell death. **A,** Model of Sr35 protein
621 with amino acid numbers used to delineate the boundaries of domains and/or motifs listed below.
622 CC = coiled-coil, NB = nucleotide binding, NB-ARC =nucleotide binding adaptor, and LRR =
623 leucine-rich repeat. Sr35 wild-type (WT) protein and its truncated variants are shown below the
624 model. **B,** Macroscopic cell death in *N. benthamiana* leaves 48 hpi with Sr35 and its truncated
625 variants. All proteins were C-terminally tagged with GFP. ev refers to empty vector. **C,**
626 Electrolyte leakage was monitored from 20 to 50 hpi. Error bars correspond to standard error
627 based on four biological replicates per construct. Different letters represent significantly different
628 groups of means based on Tukey's HSD test (α = 0.01) performed at the last time point
629 (statistical analyses in Supplementary Table S3). **D,** GFP-HRP Western blot showing proteins
630 expressed at expected sizes for all constructs. GFP cleavage* was observed in CC, NB, and CC-

NB constructs. The lower panel is the same blot stained with Ponceau S to reveal bands corresponding to Rubisco's large subunit protein as loading control.

Figure 3. Sr35 CC-NB-ARC D503V induces strong cell death. **A,** Model of Sr35 protein with the amino acid numbers used to delineate the boundaries of domains and/or motifs listed below. CC = coiled-coil, NB = nucleotide binding, NB-ARC =nucleotide binding adaptor, and LRR = leucine-rich repeat. The D503V auto-active mutation is marked above the model. Truncation variants used in this experiment are shown below. **B,** Macroscopic cell death in *N. benthamiana* leaves 48 hpi with *Agrobacterium*. ev refers to empty vector construct. **C,** Electrolyte leakage for all constructs was monitored 20 to 50 hpi. Error bars represent standard error based on four biological replicates per construct. Different letters represent significantly different groups of means based on Tukey's HSD test ($\alpha = 0.01$) performed at the last time point (statistical analyses in Supplementary Table S4). **D,** GFP-HRP Western blot showing that all constructs, except Sr35 D503V-GFP, expressed proteins of the expected sizes. Sr35 D503V-GFP was detected by immunoprecipitation (Supplementary Figure S2). Relatively weak protein expression was noted for all constructs with the D503V auto-active mutation. The lower panel is the same blot stained with Ponceau S to reveal bands corresponding to Rubisco's large subunit protein as loading control.

Figure 4. Transient expression of *Sr35* constructs in barley. Top panel: macroscopic cell death in Manchuria barley leaves 7 days post infiltration with *Agrobacterium* carrying *Sr35* constructs. Ratios represent the number of the 20 leaves transformed with each construct that showed the same result as the presented images. Lower panel: macroscopic cell death in *Nicotiana*

653 *benthamiana* leaves 48 hpi with the same *Agrobacterium* culture. Leaf images were cropped to
654 save space. The entire experiment was repeated twice with similar results.

655 **Figure 5**. AvrSr35 and Sr35 with a C-terminal GFP tag trigger a strong cell death response. **A,**
656 Schematic diagram of *Sr35* and *AvrSr35* constructs. **B,** Macroscopic cell death in *N.*
657 *benthamiana* leaves 48 hpi with *Agrobacterium* (+ indicates co-infiltration). Avr refers to the
658 AvrSr35-SP+mRFP construct (no signal peptide and mRFP C-terminal tag). Avr+Avr co-
659 infiltration control corresponds to AvrSr35 infiltrated at double the optical density. **C,** Electrolyte
660 leakage for all constructs was monitored from 20 to 50 hpi. Error bars represent standard error
661 based on four biological replicates per construct. Different letters represent significantly different
662 groups of means based on Tukey's HSD test ($\alpha = 0.01$) performed at the last time point
663 (statistical analyses in Supplementary Table S6). **D,** GFP-HRP Western blot (upper panel)
664 showing that all constructs except Sr35 D503V-GFP expressed proteins of the expected sizes.
665 Sr35 D503V-GFP was detected by immunoprecipitation (Supplementary Fig. S2). The blot
666 shown below is the same blot stained with Ponceau S to reveal bands corresponding to Rubisco's
667 large subunit protein as a loading control. DsRed; Mouse-HRP Western Blot (lower panel)
668 showing AvrSr35 in all co-infiltrated samples except Avr+Sr35 D503V-GFP, likely due to rapid
669 cell death. The blot shown below is the same blot stained with Ponceau S to reveal bands
670 corresponding to Rubisco's large subunit protein as loading control.

671 **Figure 6**. AvrSr35 recognition by Sr35 in barley. **A,** Model of AvrSr35-SP+HA (no signal
672 peptide and C-terminal HA tag) construct. **B,** Transient expression of Sr35 and AvrSr35-SP+HA
673 constructs in barley. Top panel: macroscopic cell death in Manchuria barley leaves 7 days post
674 infiltration with *Agrobacterium* carrying Sr35 and AvrSr35-SP+HA constructs. Ratios represent
675 the number of the 20 leaves transformed with each construct that showed the same result as the

presented images. Lower panel: macroscopic cell death in *Nicotiana benthamiana* leaves 72 hpi with the same *Agrobacterium* culture. Leaf images were cropped to save space. The experiment was repeated twice with similar results. **C,** HA-HRP Western Blot (upper panel) showing AvrSr35-SP+HA expressed at the expected size in *N. benthamiana*. ev = empty vector. The blot was also stained with Ponceau S (lower panel) to reveal bands corresponding to Rubisco's large subunit protein as a loading control.

Supplementary Figures

Supplementary Figure S1. The addition of a C-terminal GFP tag did not alter the induction of cell death by the Sr35 CC domain and the Sr35 complete protein in *N. benthamiana.* **A,** Models of the Sr35 CC domain and the complete Sr35 protein with and without a GFP tag. The CC domain corresponds to the first 155 amino acids of Sr35 protein. **B,** Macroscopic cell death observed in *N. benthamiana* leaves 48 hpi with *Agrobacterium*. CC = coiled-coil, WT= wild-type, GFP= green fluorescent protein.

Supplementary Figure S2. Auto-active (D503V) full-length Sr35 proteins were expressed at the expected size. Protein was extracted from *N. benthamiana* leaves 24 hpi. Sr35 D503V auto-active and C319A/C649A/D503V constructs with C-terminal GFP tags were immunoprecipitated with GFP-Trap beads. The blot was stained with Ponceau S (below) to reveal bands corresponding to Rubisco's large subunit protein as loading control. ev = empty vector; L = loading control sample; E = GFP immunoprecipitation elution. A cross-reacting band* was observed around 17kDa in the ev elution.

Supplementary Figure S3. Mutation of predicted palmitoylation sites in Sr35 did not affect the induction of cell death. **A,** Model of Sr35 protein with the amino acid numbers used to delineate the domains and/or motifs listed below. CC = coiled-coil, NB = nucleotide binding, NB-ARC = nucleotide binding adaptor, and LRR = leucine-rich repeat. Positions of auto-active mutation D503V, P-loop mutation K206R, and predicted palmitoylation site mutations C319A and C649A are marked above the model. **B,** Macroscopic cell death observed when Sr35 WT and its mutants were transiently expressed in *Nicotiana benthamiana.* Leaves were imaged 48 hpi with *Agrobacterium*. All proteins were C-terminally tagged with GFP. ev = empty vector construct. **C,** Electrolyte leakage for all constructs was monitored from 15 to 45 hpi. Error bars represent standard error based on four biological replicates per construct. Different letters indicate significantly different groups of means based on Tukey's HSD test ($\alpha = 0.01$) performed at the last time point (statistical analyses in Supplementary Table S5). **D,** GFP-HRP Western blot showing that all constructs expressed proteins of the expected sizes. 20µg of protein extracted from *N. benthamiana* tissue at 24 hpi was analyzed for each sample. No protein was observed for both Sr35 D503V-GFP and Sr35 C319A/C649A/D503V, presumably due to strong cell death induced by these constructs at this time point. However, these proteins were detected after immunoprecipitation (Supplementary Fig. S2). The blot was also stained with Ponceau S (below) to reveal bands corresponding to Rubisco's large subunit protein as loading control.

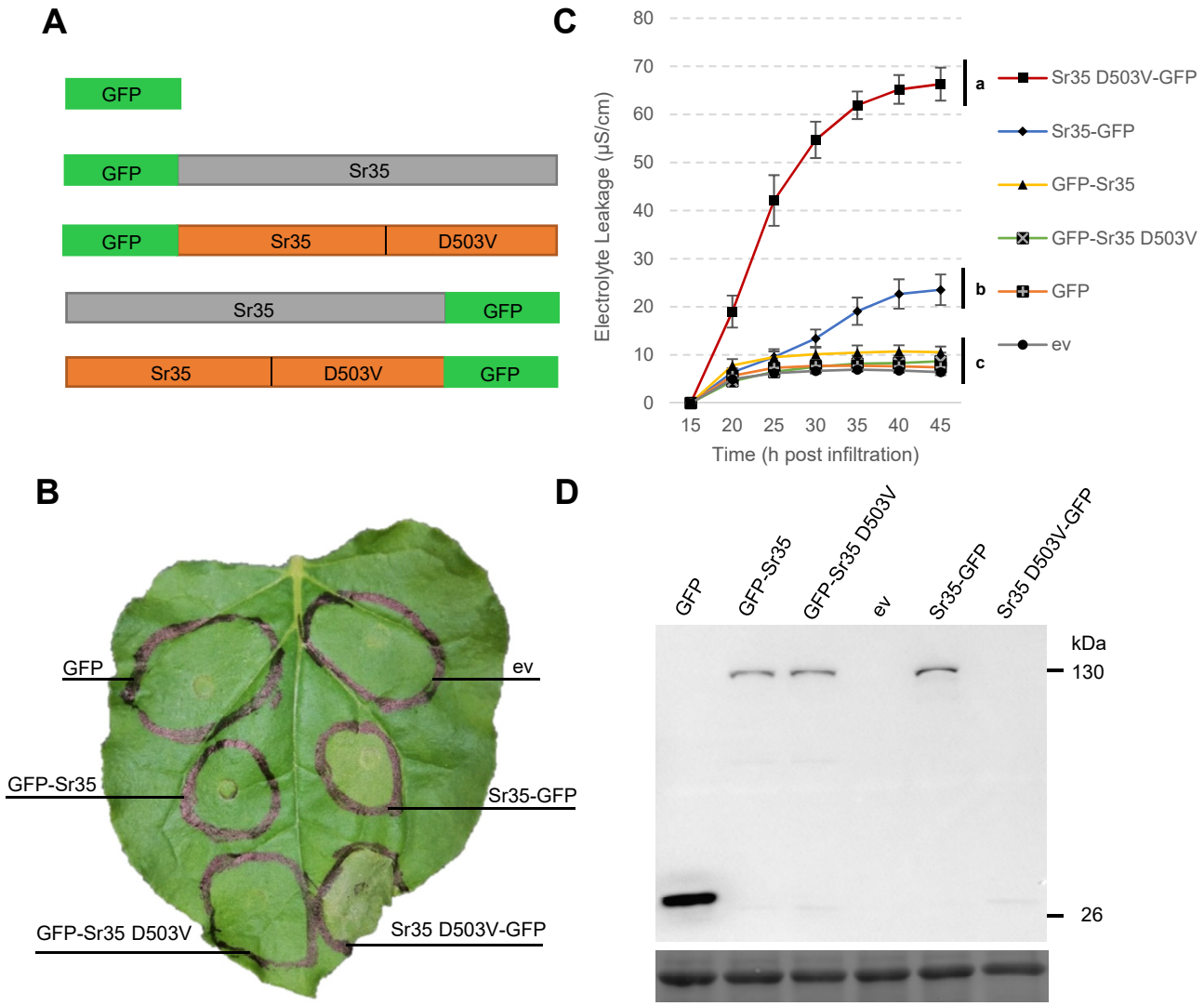
A
GFP
GFP
Sr35
GFP
Sr35
D503V
Sr35
GFP
Sr35
D503V
GFP
B
GFP
ev
GFP-Sr35
Sr35-GFP
GFP-Sr35 D503V
Sr35 D503V-GFP
C
Electrolyte Leakage (µS/cm)
Time (h post infiltration)
Sr35 D503V-GFP
Sr35-GFP
GFP-Sr35
GFP-Sr35 D503V
GFP
ev
a
b
c
D
GFP
GFP-Sr35
GFP-Sr35 D503V
ev
Sr35-GFP
Sr35 D503V-GFP
kDa
130
26

Figure 1

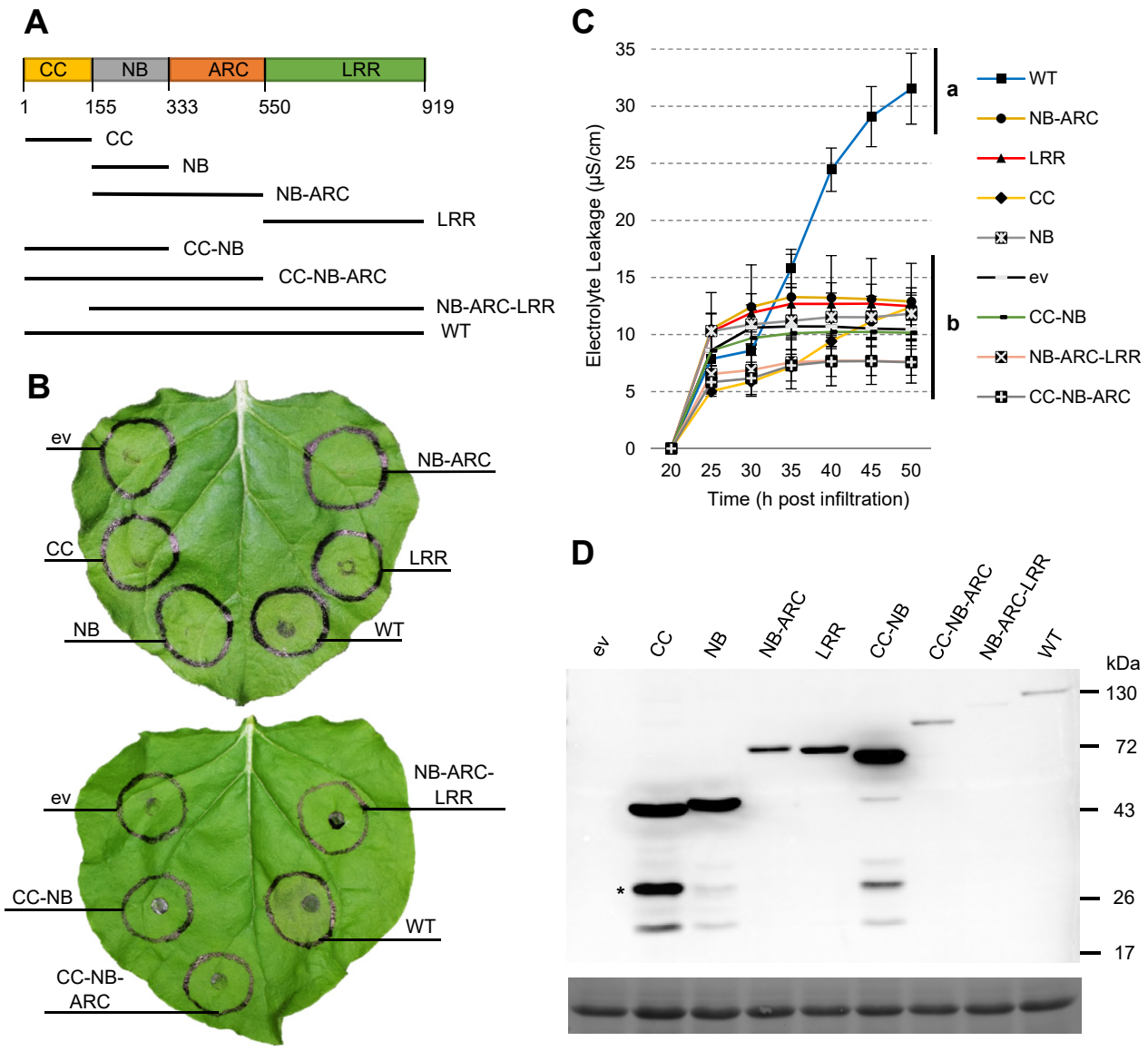
A
CC
NB
ARC
LRR
1
155
333
550
919
CC
NB
NB-ARC
LRR
CC-NB
CC-NB-ARC
NB-ARC-LRR
WT
B
ev
NB-ARC
CC
LRR
NB
WT
ev
NB-ARC-LRR
CC-NB
WT
CC-NB-ARC
C
Electrolyte Leakage (µS/cm)
Time (h post infiltration)
a
b
WT
NB-ARC
LRR
CC
NB
ev
CC-NB
NB-ARC-LRR
CC-NB-ARC
D
ev
CC
NB
NB-ARC
LRR
CC-NB
CC-NB-ARC
NB-ARC-LRR
WT
kDa
130
72
43
26
17
*

Figure 2

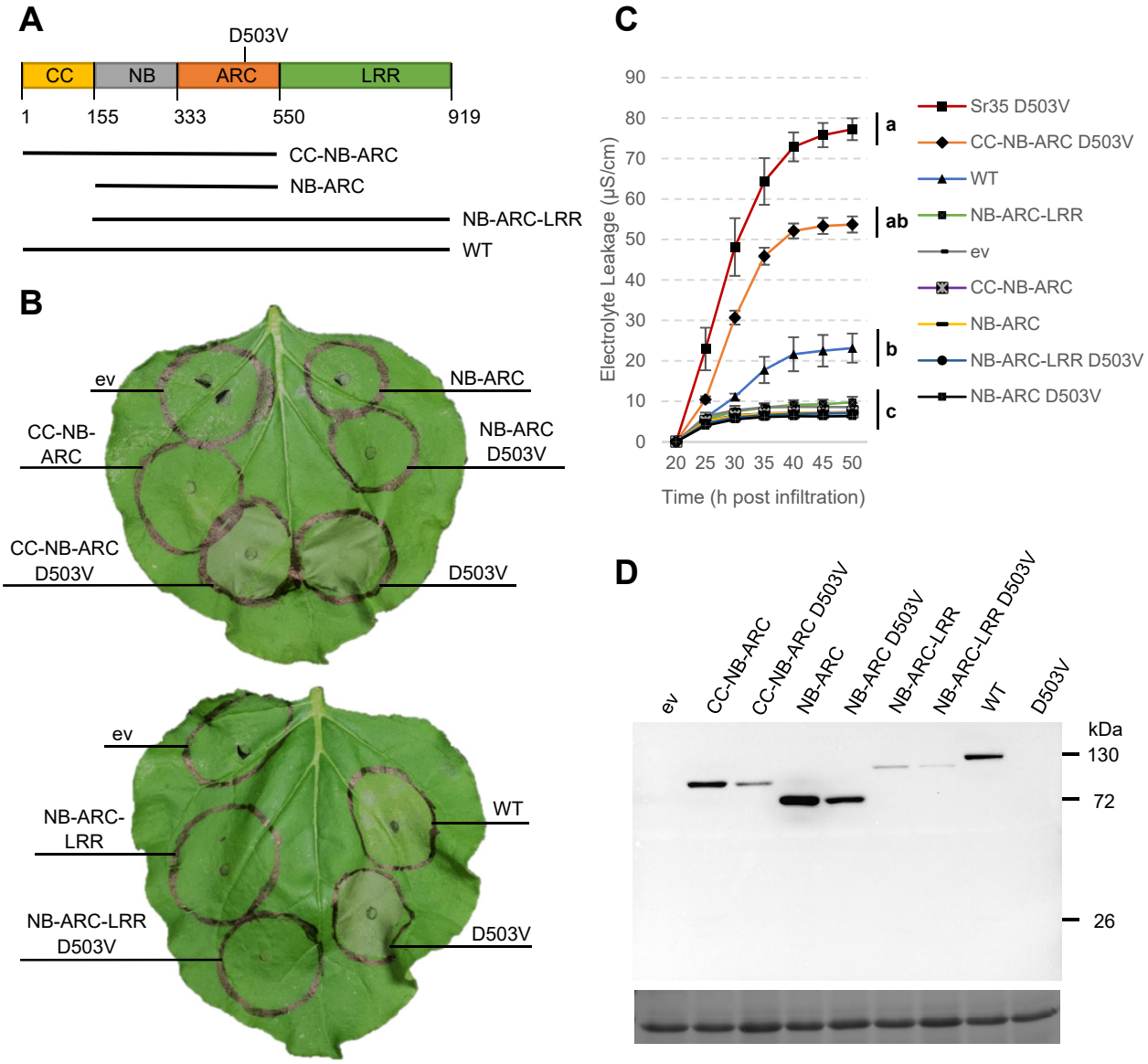
A
D503V
CC
NB
ARC
LRR
1
155
333
550
919
CC-NB-ARC
NB-ARC
NB-ARC-LRR
WT
B
ev
NB-ARC
CC-NB-ARC
NB-ARC D503V
CC-NB-ARC D503V
D503V
ev
WT
NB-ARC-LRR
NB-ARC-LRR D503V
D503V
C
Electrolyte Leakage (µS/cm)
Time (h post infiltration)
a
ab
b
c
Sr35 D503V
CC-NB-ARC D503V
WT
NB-ARC-LRR
ev
CC-NB-ARC
NB-ARC
NB-ARC-LRR D503V
NB-ARC D503V
D
ev
CC-NB-ARC
CC-NB-ARC D503V
NB-ARC
NB-ARC D503V
NB-ARC-LRR
NB-ARC-LRR D503V
WT
D503V
kDa
130
72
26

Figure 3

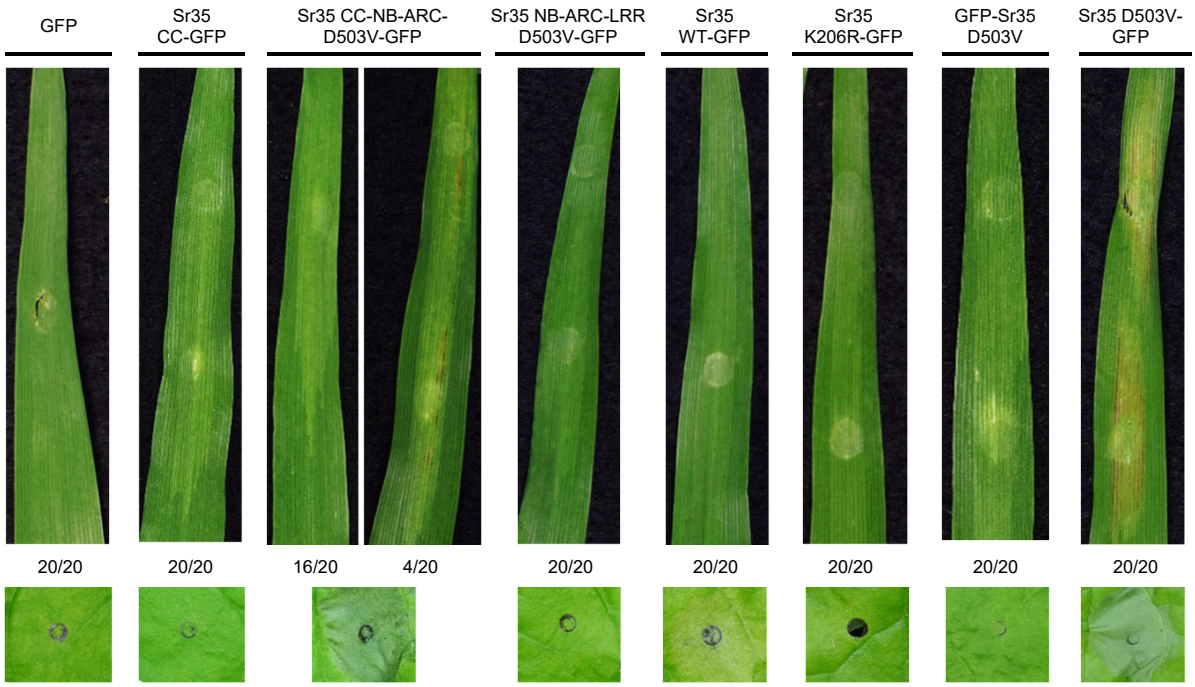
GFP
Sr35 CC-GFP
Sr35 CC-NB-ARC-D503V-GFP
Sr35 NB-ARC-LRR D503V-GFP
Sr35 WT-GFP
Sr35 K206R-GFP
GFP-Sr35 D503V
Sr35 D503V-GFP
20/20
20/20
16/20
4/20
20/20
20/20
20/20
20/20
20/20

Figure 4

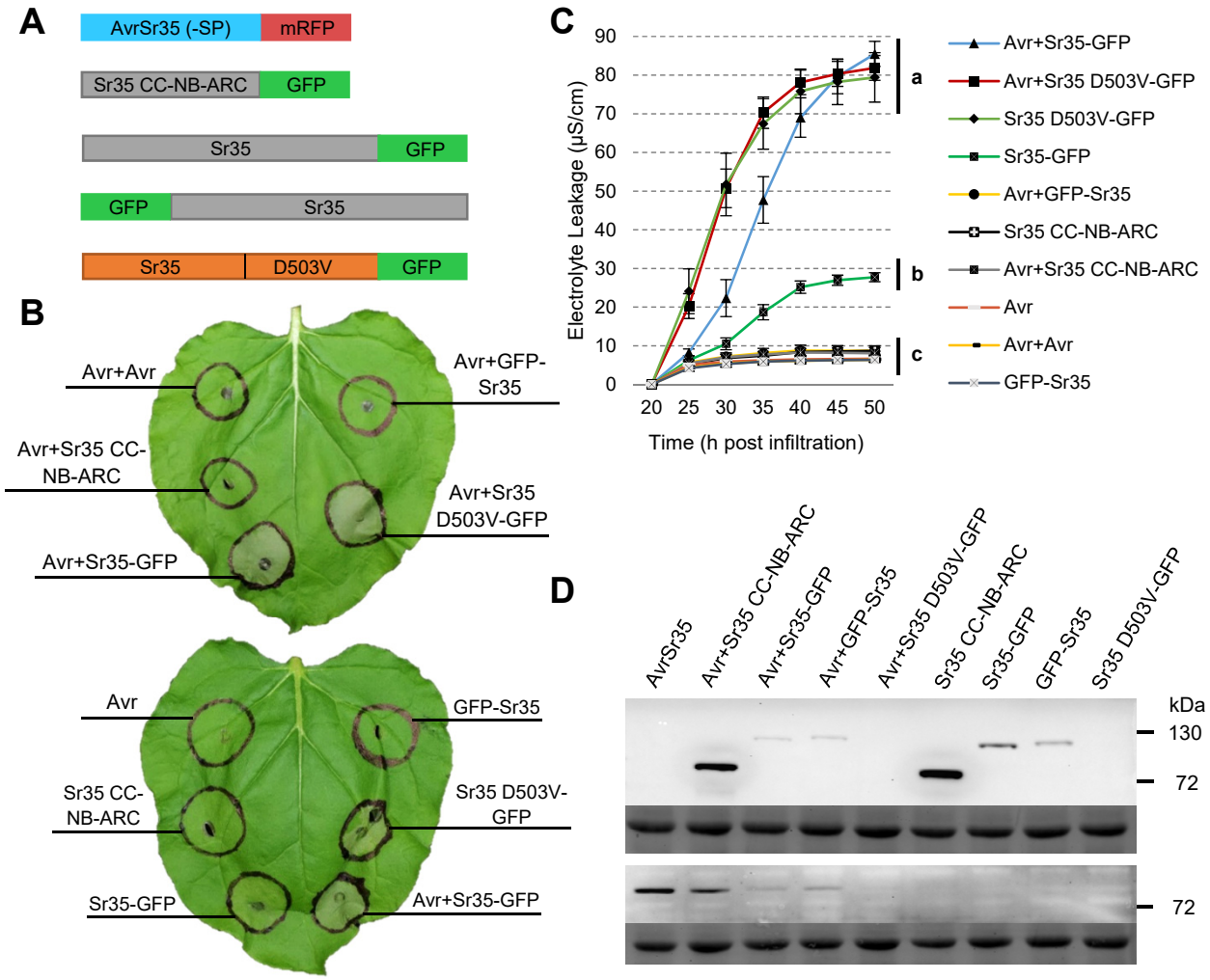
A
AvrSr35 (-SP)
mRFP
Sr35 CC-NB-ARC
GFP
Sr35
GFP
GFP
Sr35
Sr35
D503V
GFP
B
Avr+Avr
Avr+GFP-Sr35
Avr+Sr35 CC-NB-ARC
Avr+Sr35 D503V-GFP
Avr+Sr35-GFP
Avr
GFP-Sr35
Sr35 CC-NB-ARC
Sr35 D503V-GFP
Sr35-GFP
Avr+Sr35-GFP
C
Electrolyte Leakage (µS/cm)
Time (h post infiltration)
a
b
c
Avr+Sr35-GFP
Avr+Sr35 D503V-GFP
Sr35 D503V-GFP
Sr35-GFP
Avr+GFP-Sr35
Sr35 CC-NB-ARC
Avr+Sr35 CC-NB-ARC
Avr
Avr+Avr
GFP-Sr35
D
AvrSr35
Avr+Sr35 CC-NB-ARC
Avr+Sr35-GFP
Avr+GFP-Sr35
Avr+Sr35 D503V-GFP
Sr35 CC-NB-ARC
Sr35-GFP
GFP-Sr35
Sr35 D503V-GFP
kDa
130
72
72

Figure 5

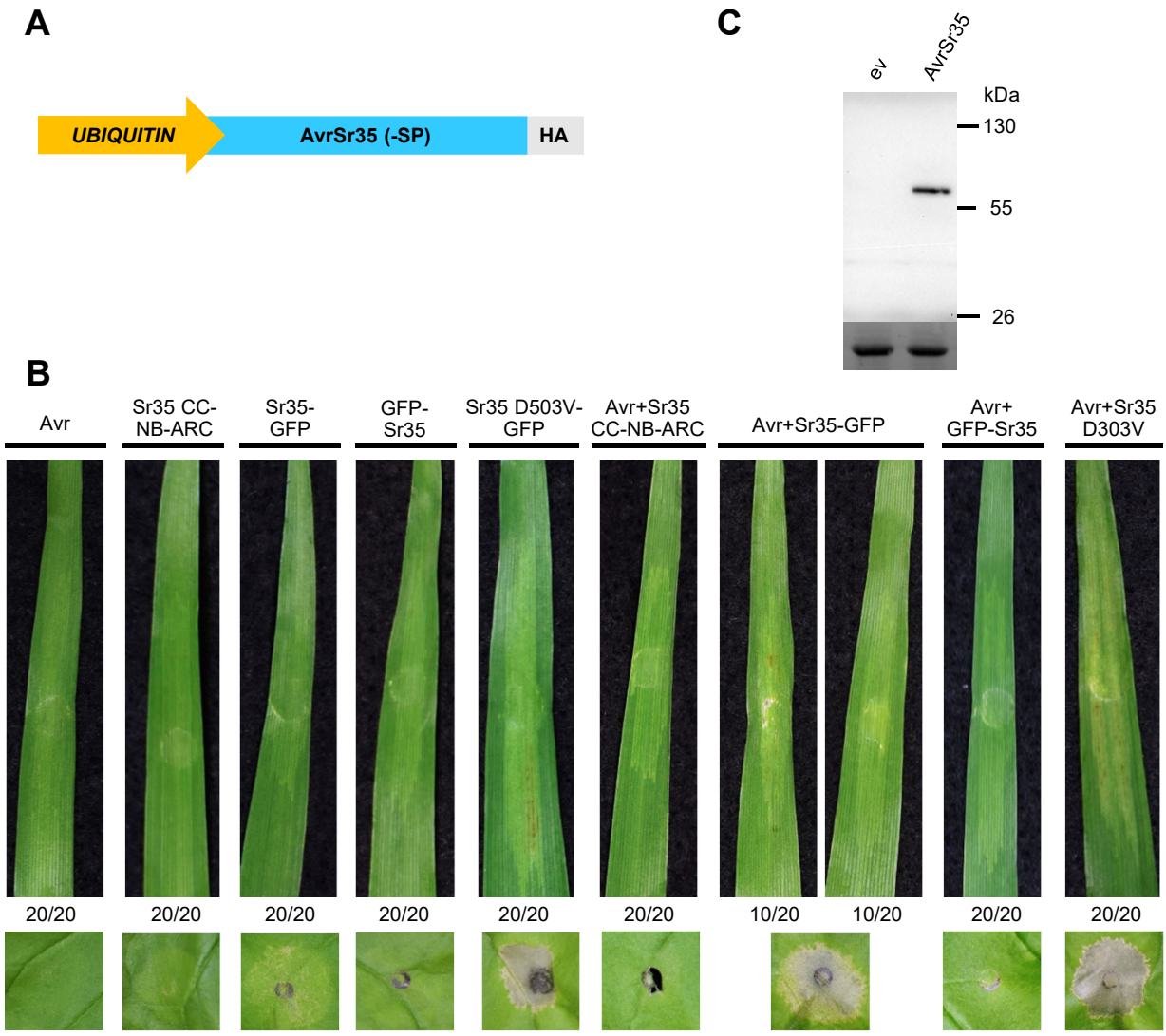
A
UBIQUITIN
AvrSr35 (-SP)
HA
C
ev
AvrSr35
kDa
130
55
26
B
Avr
Sr35 CC-NB-ARC
Sr35-GFP
GFP-Sr35
Sr35 D503V-GFP
Avr+Sr35 CC-NB-ARC
Avr+Sr35-GFP
Avr+GFP-Sr35
Avr+Sr35 D303V
20/20
20/20
20/20
20/20
20/20
20/20
10/20
10/20
20/20
20/20

Figure 6

Supplementary Tables

Supplementary Table S1. Primers used in this study.

Primer Name	Primer sequence 5' to 3'
Sr35gateway_F	GGGGACAAGTTTGTACAAAAAAGCAGGCTTCATGGAGATTGCCATGGGG
Sr35gateway_R	GGGGACCACTTTGTACAAGAAAGCTGGGTCCCATATATCGAGGATGGG
Sr35CCgateway_R	GGGGACCACTTTGTACAAGAAAGCTGGGTCGTCAACACTAGTATTAGC
Sr35NBgateway_F	GGGGACAAGTTTGTACAAAAAAGCAGGCTTCATGCCTCGCATGATGGCCTTG
Sr35NBgateway_R	GGGGACCACTTTGTACAAGAAAGCTGGGTCGGAAAGGGGTTCCATCCT
Sr35ARCgateway_R	GGGGACCACTTTGTACAAGAAAGCTGGGTCGGTATCCACATCTATCTT
Sr35LRRgateway_F	GGGGACAAGTTTGTACAAAAAAGCAGGCTTCATGACTAGGATGGAGCATATG
Sr35C319A_F	GTTAGTGTCTCTGAAGCAGCTTGCTCTTCTGAGGATG
Sr35C319A_R	CATCCTCAGAAGAGCAAGCTGCTTCAGAGACACTAAC
Sr35C649A_F	CAACTAAGACGTCTAATGGCTCTGTATGTTGATTATG
Sr35C649A_R	CATAATCAACATACAGAGCCATTAGACGTCTTAGTTG
Sr35D503V_F	GCTTGCCGTGTACATGTTATGGTGCTTGACCTC
Sr35D503V_R	GAGGTCAAGCACCATAACATGTACACGGCAAGC
Sr35K206R_F	GTGGGTTAGGCAGGACGACTCTTGC
Sr35K206R_R	GCAAGAGTCGTCCTGCCTAACCCAC
Sr35_TGA_gateway_R	GGGGACCACTTTGTACAAGAAAGCTGGGTCTCACCATATATCGAGGAT
Sr35CC_TGA_gateway_R	GGGGACCACTTTGTACAAGAAAGCTGGGTCTCAGTCAACACTAGTATTAGC
AvrSr35gateway_F	GGGGACAAGTTTGTACAAAAAGCAGGCTTCATGGCCATGAGGAACTTTGCTGC
AvrSr35gateway_R	GGGGACCACTTTGTACAAGAAAGCTGGGTCCAATTTGCCTTCATGAACATT

Supplementary Table S2. Statistical analysis of electrolyte leakage at 45 h by individual experiments and in a combined ANOVA using experiments as blocks. We compared all means against each other using Tukey's tests. Different letters indicate significant differences at $P < 0.01$. Results from Experiment 1 are shown in Figure 1C.

Construct	Exp. 1	$P < 0.01$	Exp. 2	$P < 0.01$	Combined	$P < 0.01$
1. Sr35:GFP D503V	66.3 ± 3.4	A	74.2 ± 3.8	A	70.2 ± 2.8	A
2. Sr35:GFP	23.5 ± 3.2	B	23.4 ± 1.8	B	23.4 ± 1.7	B
3. GFP:Sr35 D503V	8.7 ± 1.8	C	12.4 ± 1.8	BC	10.5 ± 1.4	C
4. GFP:Sr35	10.6 ± 1.2	C	11.3 ± 1.8	C	10.9 ± 1.0	C
5. GFP	7.4 ± 0.5	C	8.3 ± 0.7	C	7.9 ± 0.4	C
6. Empty vector	6.4 ± 0.6	C	9.1 ± 0.9	C	7.8 ± 0.7	C
Overall ANOVA [a]	$P < 0.0001$		$P < 0.0001$		$P < 0.0001$	

[a] A power transformation was used in the combined analysis to restore normality of residuals (Shapiro-Wilk test) and homogeneity of variances (Levene's test). Tukey *P* values are from the transformed data, but the means in the table are from untransformed data followed by the standard error of the means (s.e.m.). Individual experiments did not require transformation.

Supplementary Table S3. Sr35 truncations. Statistical analysis of electrolyte leakage at 50 h by individual experiments and in a combined ANOVA using experiments as blocks. We compared all the means against each other using Tukey's tests. Different letters indicate significant differences at $P < 0.01$. Results from Experiment 1 are shown in Figure 2C.

Construct	Exp. 1	$P < 0.01$	Exp. 2	$P < 0.01$	Combined	$P < 0.01$
1. WT	31.5 ± 3.1	A	29.8 ± 2.6	A	30.7 ± 1.9	A
2. CC	12.4 ± 1.0	B	10.4 ± 0.7	B	11.4 ± 0.7	B
3. LRR	12.5 ± 1.6	B	8.8 ± 0.7	BC	10.6 ± 1.1	B
4. NB	11.8 ± 1.8	B	8.4 ± 0.9	BC	10.1 ± 1.1	B
5. NB-ARC	12.9 ± 3.4	B	6.9 ± 0.1	BC	9.9 ± 1.9	B
6. CC-NB	10.1 ± 1.1	B	6.4 ± 0.8	BC	8.3 ± 1.0	B
7. NB-ARC-LRR	7.6 ± 1.8	B	8.5 ± 0.8	BC	8.0 ± 0.9	B
8. CC-NB-ARC	7.6 ± 1.1	B	5.5 ± 0.8	C	6.6 ± 0.7	B
9. Empty vector	10.4 ± 0.8	B	4.9 ± 0.7	C	7.7 ± 1.2	B
Overall ANOVA [a]	$P < 0.0001$		$P < 0.0001$		$P < 0.0001$	

[a] A square root transformation was used to restore normality of residuals (Shapiro-Wilk test) and homogeneity of variances (Levene's test) in the combined analysis and in Experiment 2. Tukey *P* values are from the transformed data, but all the means in the table are from untransformed data followed by s.e.m. Experiment 1 did not require transformation.

Supplementary Table S4. Sr35 auto-active mutant truncations. Statistical analysis of electrolyte leakage at 50 h by individual experiments and in a combined ANOVA using experiments as blocks. We compared all the means against each other using Tukey's tests. Different letters indicate significant differences at $P < 0.01$. Results from Experiment 1 are shown in Figure 3C.

Construct	Exp. 1	$P < 0.01$	Exp. 2	$P < 0.01$	Combined	$P < 0.01$
1. Complete D503V	77.3 ± 2.7	A	77.5 ± 5.6	A	77.4 ± 2.9	A
2. CC-NB-ARC D503V	53.7 ± 2.0	AB	56.5 ± 6.7	AB	55.1 ± 3.3	A
3. WT	23.1 ± 3.6	B	35.1 ± 4.5	B	29.1 ± 3.5	B
4. NB-ARC-LRR	9.7 ± 1.4	C	11.6 ± 1.7	C	10.7 ± 1.1	C
5. Empty vector	8.5 ± 1.1	C	7.3 ± 0.8	C	7.9 ± 0.7	CD
6. NB-ARC-LRR D503V	7.0 ± 0.5	C	8.5 ± 0.8	C	7.8 ± 0.5	CD
7. CC-NB-ARC	7.3 ± 1.2	C	8.3 ± 0.4	C	7.8 ± 0.6	CD
8. NB-ARC	7.2 ± 0.6	C	7.0 ± 0.3	C	7.1 ± 0.3	D
9. NB-ARC D503V	6.3 ± 0.3	C	6.6 ± 0.1	C	6.5 ± 0.2	D
Overall ANOVA [a]	$P < 0.0001$		$P < 0.0001$		$P < 0.0001$	

[a] A power transformation was used to restore normality of residuals (Shapiro-Wilk test) and homogeneity of variances (Levene's test) for the ANOVA. Tukey *P* values are from the transformed data, but all the means in the table are from untransformed data followed by s.e.m.

Supplementary Table S5. Sr35 wild type and auto-active mutants with and without mutations C319A and C649A in putative palmitoylation sites. Statistical analysis of electrolyte leakage at 45 h by individual experiments and in a combined ANOVA using experiments as blocks. We compared all the means against each other using Tukey's tests. Different letters indicate significant differences at $P < 0.01$. Results from Experiment 1 are shown in Supplementary Figure S3C.

Construct	Exp. 1	$P < 0.01$	Exp. 2	$P < 0.01$	Combined	$P < 0.01$
1. Sr35:GFP D503V	66.3 ± 3.4	A	77.6 ± 4.7	A	71.9 ± 3.4	A
2. $Sr35_{C319A/C649A}$:GFP D503V	61.2 ± 5.0	A	72.7 ± 3.7	A	66.9 ± 3.6	A
3. Sr35:GFP	23.5 ± 3.2	B	24.7 ± 4.3	B	24.1 ± 2.5	B
4. $Sr35_{C319A/C649A}$:GFP	20.9 ± 1.6	B	17.7 ± 2.7	B	19.3 ± 1.5	B
5. $Sr35_{K206R}$:GFP	8.7 ± 1.8	C	5.8 ± 0.7	C	7.3 ± 1.1	C
6. Empty vector	6.4 ± 0.6	C	5.0 ± 0.4	C	5.7 ± 0.4	C
ANOVA [a]	$P < 0.0001$		$P < 0.0001$		$P < 0.0001$	

[a] A square root transformation was used to restore normality of residuals (Shapiro-Wilk test) and homogeneity of variances (Levene's test) in all ANOVAs. Tukey *P* values are from the transformed data, but all the means in the table are from untransformed data followed by s.e.m.

Supplementary Table S6. Sr35 and AvrSr35 co-infiltrations. Statistical analysis of electrolyte leakage at 50 h by individual experiments and in a combined ANOVA using experiments as blocks. We compared all the means against each other using Tukey's tests. Different letters indicate significant differences at $P < 0.01$. Avr= AvrSr35-SP+mRFP (effector without the signal peptide and with a C-terminal monomeric Red Fluorescent Protein tag). Results from Experiment 2 are shown in Figure 5C.

Construct	Exp. 1	$P < 0.01$	Exp. 2	$P < 0.01$	Combined	$P < 0.01$
1. Avr + Sr35:GFP	65.7 ± 1.3	A	85.5 ± 3.2	A	75.6 ± 4.1	A
2. Avr + Sr35:GFP D503V	69.1 ± 7.4	A	81.9 ± 3.2	A	75.5 ± 4.5	A
3. Sr35:GFP D503V	68.6 ± 1.0	A	79.4 ± 6.4	A	74.0 ± 3.6	A
4. Sr35:GFP	23.1± 1.7	B	27.7 ± 1.2	B	25.4 ± 1.3	B
5. Avr + Sr35CCNBARC	10.9 ± 0.6	C	8.1 ± 0.5	C	9.5 ± 0.7	C
7. Avr + Avr[a]	9.3 ± 0.6	CD	6.4 ± 0.8	C	7.9 ± 0.7	C
6. Avr + GFP:Sr35	8.4 ± 1.5	CD	8.7 ± 1.3	C	8.5 ± 0.9	C
8. Sr35 CCNBARC	6.8 ± 0.7	CD	8.7 ± 0.9	C	7.7 ± 0.6	C
9. Avr	6.9 ± 0.5	CD	6.6 ± 0.8	C	6.8 ± 0.4	C
10. GFP:Sr35	6.4 ± 0.6	D	6.4 ± 0.5	C	6.4 ± 0.4	C
Overall ANOVA[b]	$P < 0.0001$		$P < 0.0001$		$P < 0.0001$	

[a] Avr+Avr co-infiltration control corresponds to AvrSr35 infiltrated at double the optical density of Avr.

[b] A log+1 transformation was used to restore normality of residuals (Shapiro-Wilk test) and homogeneity of variances (Levene's test) in all the ANOVAs. Tukey *P* values are from the transformed data, but all the means in the table are from untransformed data followed by s.e.m.

Supplementary Figure S1. The addition of a C-terminal GFP tag did not alter the induction of cell death by the Sr35 CC domain and the Sr35 complete protein in *N. benthamiana.* **A,** Models of the Sr35 CC domain and the complete Sr35 protein with and without a GFP tag. The CC domain corresponds to the first 155 amino acids of Sr35 protein. **B,** Macroscopic cell death observed in *N. benthamiana* leaves 48 hpi with *Agrobacterium*. CC = coiled-coil, WT= wild-type, GFP= green fluorescent protein.

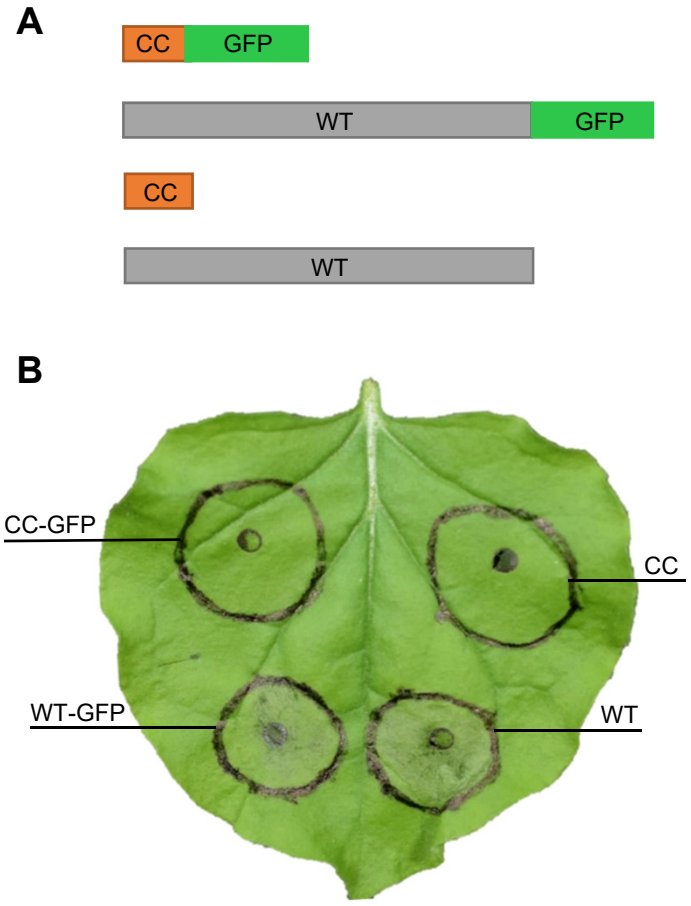

Supplementary Figure S2. Auto-active (D503V) full-length Sr35 proteins were expressed at the expected size. Protein was extracted from *N. benthamiana* leaves 24 hpi. Sr35 D503V auto-active and C319A/C649A/D503V constructs with C-terminal GFP tags were immunoprecipitated with GFP-Trap beads. The blot was stained with Ponceau S (below) to reveal bands corresponding to Rubisco's large subunit protein as loading control. ev = empty vector; L = loading control sample; E = GFP immunoprecipitation elution. A cross-reacting band* was observed around 17 kDa in the "ev" elution.

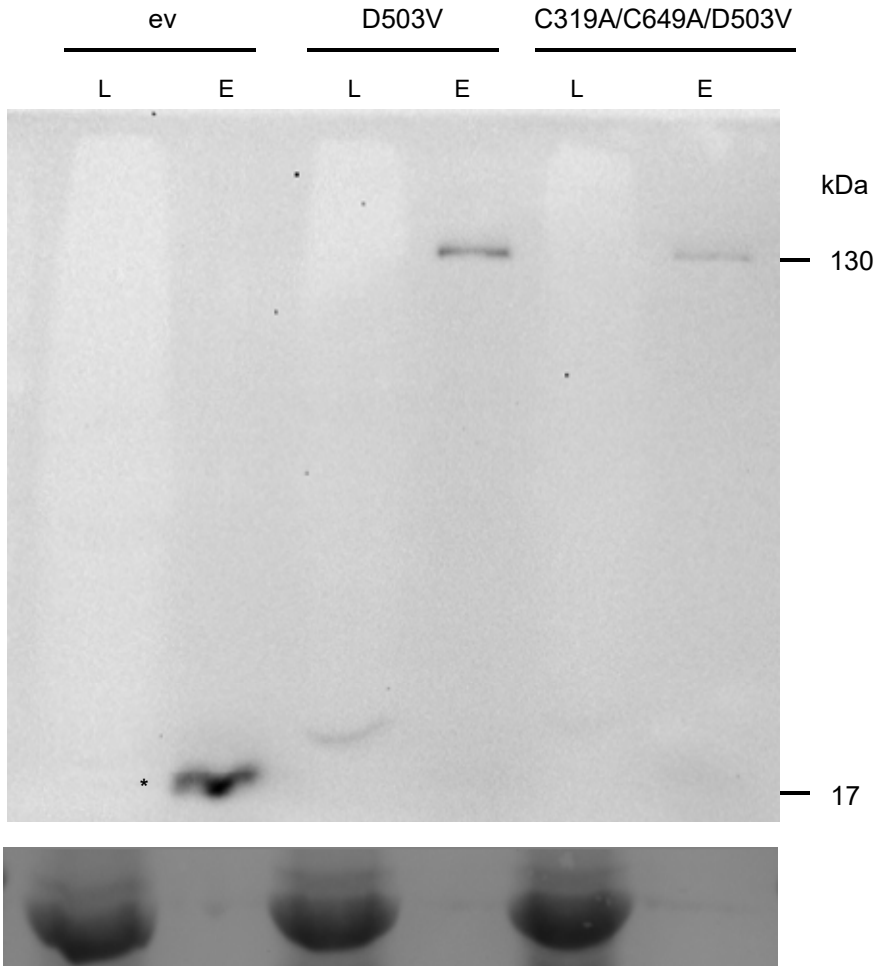

Supplementary Figure S3. Mutation of predicted palmitoylation sites in Sr35 did not affect induction of cell death. **A,** Model of Sr35 protein with amino acid numbers used to delineate the domains and/or motifs. CC = coiled-coil, NB = nucleotide binding, NB-ARC = nucleotide binding adaptor, and LRR = leucine-rich repeat. Positions of auto-active mutation D503V, P-loop mutation K206R, and predicted palmitoylation site mutations C319A and C649A are marked above the model. **B,** Macroscopic cell death observed when Sr35 WT and its mutants were transiently expressed in *Nicotiana benthamiana.* Leaves were imaged 48 hpi with *Agrobacterium*. All proteins were C-terminally tagged with GFP. ev = empty vector construct. **C,** Electrolyte leakage for all constructs was monitored from 15 to 45 hpi. Error bars represent standard error based on four biological replicates per construct. Different letters indicate significantly different groups of means based on Tukey's HSD test ($\alpha = 0.01$) performed at the last time point (statistical analyses in Supplementary Table S5). **D,** GFP-HRP Western blot showing that all constructs expressed proteins of the expected sizes. 20µg of protein extracted from *N. benthamiana* tissue at 24 hpi was analyzed for each sample. No protein was observed for both Sr35 D503V-GFP and Sr35 C319A/C649A/D503V (these proteins were detected after immunoprecipitation, Supplementary Fig. S2). The control blot below was stained with Ponceau S (Rubisco's large subunit protein).